HOKKAIDO UNIVERSITY

Title	Two Stabiliser loci suppress Tam3 transposition without compromising transposase production in Antirrhinum
Author(s)	Wang, Shasha; Uchiyama, Takako; Kuwabara, Hiroyuki et al.
Citation	Plant physiology, 199(2) https://doi.org/10.1093/plphys/kiaf396
Issue Date	2025-10-01
Doc URL	https://hdl.handle.net/2115/98329
Rights	This is a pre-copyedited, author-produced version of an article accepted for publication in Plant physiology following peer review. The version of record Shasha Wang, Takako Uchiyama, Hiroyuki Kuwabara, Megumi Hirata, Ikumi Yuasa, Kenji Nakahara, Cathie Martin, Yuji Kishima, Two Stabiliser loci suppress Tam3 transposition without compromising transposase production in Antirrhinum, Plant Physiology, Volume 199, Issue 2, October 2025, is available online at: https://doi.org/10.1093/plphys/kiaf396.
Type	journal article
File Information	Wang et al. Plant Physiology 2025.pdf

Hokkaido University Collection of Scholarly and Academic Papers : HUSCAP

Two *Stabiliser* loci in *Antirrhinum* suppress the transposition of Tam3 without compromising transposase production.

Shasha Wang [1], Takako Uchiyama [1], Hiroyuki Kuwabara [1], Megumi Hirata [1], Ikumi Yuasa [1], Kenji Nakahara [1], Cathie Martin [2], Yuji Kishima [1*]

1: Research Faculty of Agriculture, Hokkaido University, Sapporo 060-8589, Japan

2: Department of Metabolic Biology, John Innes Centre, Norwich, NR4 7UH, UK

* Corresponding author: Yuji Kishima (E-mail: kishima@agr.hokudai.ac.jp)

Running head: *Stabilisers* for transposon Tam3 in *Antirrhinum*

Abstract

Antirrhinum majus has been known to exhibit occasional instabilities that are manifested as variegations and morphological chimeras. *Stabiliser* (*St*) is a historical locus that stabilizes phenotypically unstable or mutable traits in *Antirrhinum*. Here, we characterized two *St* loci, the previously described *Old Stabiliser* (*OSt*) and *New Stabiliser* (*NSt*), in *Antirrhinum* that specifically suppress the transposition of the Class II DNA transposable element, Tam3. Both *St* loci involve derivatives of Tam3 with unique structures: *OSt* has a pseudo-Tam3 copy whose 5'-terminal region has been rearranged compared to the cognate Tam3 element, and *NSt* consists of two intact copies of Tam3 in a head-to-head orientation. Neither locus interferes with the production of the intact Tam3 transposase (TPase) or the nuclear import of TPase. Both *OSt* and *NSt* produce specific sRNAs from their 5' terminal regions containing multiple TPase binding motifs. We performed sRNA induction experiments by TRV-mediated virus-induced gene silencing targeting the 5’ terminal region in the Tam3 sequence, which suppressed the Tam3 transposition of the *ost*/*nst* plants. These results suggest that specific sRNAs could repress Tam3 transposition by interacting with the TPase binding motifs within the Tam3 element or with the TPase itself.

Abbreviations

Stabiliser (*St*), *Old Stabiliser* (*OSt*), *New Stabiliser* (*NSt*), Tam3 transposase (Tam3 TPase), small RNAs (sRNAs), transposable element (TE), master regulators (MRs), *Palllida* (*pal*), *Nivea* (*niv*), BED zinc finger motif (Znf-BED), open reading frame (ORF), long non-coding RNA (lncRNA), DICER-LIKE (DCL).

Introduction

The parasitism of transposable elements (TEs) as selfish genetic elements within their host organisms has been accompanied by evolution of a comprehensive set of master regulators (MRs) that control transposition of collective TEs in an epigenetic manner, inactivating the transcription of their genes and suppressing the production of the enzymes that catalyze transposition (Levin and Moran, 2011; Viviani et al., 2021; Liu et al., 2022). Consequently, few transcription or translation products are generally detected in hosts with inactivated TEs. However, some DNA transposons remain "surreptitiously" active even in repressive genomic environments. Examples of active plant DNA transposons are Ac/Ds, En/Spm, Mu in maize, Dart in rice, Tpn in morning glory, and Tam in *Antirrhinum* (Coen et al., 1989; Fedoroff et al., 1989; Inagaki et al., 1994; Gierl, 1996; Lisch, 2002; Fujino et al., 2005; Walbot and Rudenko, 2007; Lazarow et al., 2013). However, the frequency of excision of even active DNA TEs may be suppressed in response to specific host functions (Black et al., 1987; Lee et al., 1998; Slotkin et al., 2003, 2005).

Instability traits such as flower petal variegation often observed in *Antirrhinum majus* have been of interest since the 19th century. Petal variegation in *A. majus* occurring at the *Pallida* locus, which encodes dihydroflavonol 4-reductase (DFR) required for anthocyanin biosynthesis was observed by Darwin and De Vries and later referred to *palllida*^{recurrens} (*pal*^{rec}) (Coen et al., 1989). Harrison and Fincham (1964) reported that

an unlinked factor in *Antirrhinum* called *Stabiliser* (*St*) suppressed the petal variegation at *pal*^{rec}. Petal variegation at the *Nivea* (*Niv*) locus encoding chalcone synthase responsible for the *niv*^{recurrens} (*niv*^{rec}) allele and caused by Tam1 was not repressed by *St* (Harrison and Carpenter, 1973). However, a second unstable mutation in the *Nivea* locus caused by insertion of Tam3 (*niv*^{rec}:98) was strongly repressed by *St* in a semi-dominant manner (Carpenter et al., 1987). Therefore, these studies led to suggestion that *St* is able to immobilize the transpositions of any copies of Tam3 *in trans*. An additional locus, similar phenotypically to *St* that can reduce the frequency of somatic excision of Tam3 copies was identified as having arisen spontaneously in an independent lineage of the *niv*^{rec}:98 allele (Hashida et al., 2006). We renamed the historic *St* locus as *Old Stabiliser* (*OSt*) and the new locus *New Stabiliser* (*NSt*) with respect to their order of identification (Uchiyama et al., 2008).

Generally, transposition of Tam3 is not completely repressed in *A*. *majus*, but activity is regulated by temperature and is low temperature-dependent (LTDT) (Carpenter et al., 1987). The Tam3 transposase (Tam3 TPase) that catalyzes transposition is localized mainly at the plasma membrane at growth temperatures of 25°C (Fujino et al., 2011; Zhou et al., 2017). Therefore, Tam3 TPase is not present in the nucleus and cannot act on the Tam3 element in the nuclear DNA, resulting in the immobilization of Tam3 copies and the stable phenotypes associated with Tam3 unstable mutations at 25°C. Conversely at growing temperatures of 15°C, Tam3 TPase can enter to the nucleus and promote Tam3 transposition. The changes in subcellular localization of Tam3 TPase in response to temperature involved in LTDT are associated with the BED zinc finger motif (Znf-BED) of Tam3 TPase (Fujino et al., 2011; Zhou et al., 2017).

The *St* genes suppress Tam3 transposition at low temperature by mechanisms which seem to be unrelated to the processes of the TPase production (Uchiyama et al., 2008). This study addresses how the two *St* loci specifically suppress the Tam3 transposition without compromising normal Tam3 TPase function.

Results

Isolation of *OSt*

When *ost*/*niv*^{rec} (HAM2) was grown at 15℃, the petal lobes of its flowers showed strong variegation (> 1000 spots per flower) with a pale pink background due to Tam3 excision from the promoter in the *niv*^{rec} allele (Fig. 1A). PCR could detect somatic excision of Tam3 as a 2.0 kb band when *ost*/*niv*^{rec} was grown at 15℃ (Fig. 1A). Since Tam3 did not excise when grown at 25℃, no variegation of the *ost*/*niv*^{rec} petal appeared, and no excision band was detected (Fig. 1A). The 2.0 kb bands identified in *ost*/*nst*/*niv* at 15℃ and 25℃ indicated no Tam3 insertion in the wild type *Niv* allele (Supplementary Fig. 1). *OSt*/*niv*^{rec} (HAM21) shares the same *niv*^{rec} allele with *ost*/*niv*^{rec}, while *OSt* is unique (Fig. 1A). Since Tam3 activity could be monitored by the *niv*^{rec} allele even at 15°C, the weak variegation (< 20 spots per flower) observed in *OSt*/*niv*^{rec} suggested that *OSt* suppressed Tam3 transposition (Fig. 1A). PCR did not detect the 2.0 kb band for somatic excision of Tam3 from the promoter in the *niv*^{rec} allele of HAM21 when run for ≥ 30 cycles (Fig. 1A).

To confirm that *OSt* is single semi-dominant locus as described by Harrison & Fincham (Harrison and Fincham, 1968), we crossed *ost*/*niv*^{rec} (HAM2) ×*OSt*/*niv*^{rec} (HAM21). The F_2 population segregated into 118 high- and middle-spotted plants (> 100 spots per flower: we did not discriminate between high and middle spots in this population) and 35 low-spotted plants (< 20 spots per flower) (Supplementary Table 1). An independent cross was performed between *OSt*/*niv*^{rec}/*Pal* (HAM21) and *ost*/*Niv*/*pal*^{rec} (HAM22), and we selected the 51 plants possessing either homozygous *niv*^{rec} and/or homozygous *pal*^{rec} among the F_2 plants. These 51 plants segregated into 9 high- (> 500 spots per flower), 31 middle- (> 50 spots per flower) and 11 low- (< 20 spots per flower) spotted plants in the F_2 population (Supplementary Table 1). These segregations in the F_2 populations of the crosses of *OSt*/*niv*^{rec} × *ost*/*niv*^{rec} and *OSt*/*niv*^{rec}/*Pal* × *ost*/*Niv*/*pal*^{rec} statistically fitted the ratios of 3:1 and 1:2:1,

121 respectively (Supplementary Table 1 and Supplementary Fig. 2A). These segregation
122 results supported the hypothesis that the low-spotted *niv*^{rec} phenotype is regulated by a
123 single semi-dominant locus, *OSt*.
124
125 Several reports have suggested that active DNA transposons can be silenced by their
126 own, transposon-derived suppressors, and that such suppressors are produced by
127 transposon recombination, such as *KP* of the P element in *Drosophila* (Black et al.,
128 1987) and *Mu killer* (*Muk*) of the MuDR partial element in maize (Slotkin et al.,
129 2003). Thus, *OSt* might have been derived from alterations to a Tam3 element arising
130 from recombination. Supporting such an idea, Harrison & Fincham (1968) reported
131 that they observed a loss of *OSt* function somatically, in the form of higher frequency
132 of sectors on low spotted *pal*^{rec} petals. To explore this possibility, transposon tagging
133 was performed to investigate whether a specific Tam3-associated fragment exists in
134 the genome of *OSt* plants using the ORF region of Tam3 as a probe.
135
136 We obtained a 6663 bp Tam3-associated DNA restriction enzyme fragment as a
137 candidate tag for the *OSt* locus following a transposon tagging procedure (Fig. 1B and
138 Supplementary Description 1). Within this, a 3919 bp candidate *OSt*-Tam3 element
139 was located on chromosome 5 (Supplementary Fig. 3). *OSt*-Tam3 encoded a pseudo-
140 *Tam3 TPase* gene with 98.8% homology to the intact element cloned from the *Niv*
141 locus from line *niv*^{rec}:98 (Hehl et al., 1991). Notably, the 5' region of the 3919 bp *OSt*-
142 Tam3 element contained an extra 286 bp sequence caused by rearrangements of the 5'
143 end of Tam3 (Fig. 1C and Supplementary Fig. 4A). In the 5' region of the reference
144 Tam3 element, the region 1-376 bp can be divided into three parts, x-y-z. The
145 corresponding region consisting of x'-y'-z' in *OSt*-Tam3 showed 97.1% to the
146 reference element (Fig. 1C). Dot plot analysis indicated that regions x' and z' had
147 been duplicated in *OSt*-Tam3, resulting in new sequence consisting of five parts, x'-
148 y'-z'-x''-z'' (Fig. 1C and Supplementary Fig. 5A). There are 11 Tam3 TPase binding
149 GCHCG motifs in the x region of Tam3, and they are also conserved in x' and x''
150 regions of *OSt*-Tam3 (Supplementary Fig. 5B). Compared with the 5' region in intact

Tam3, the corresponding parts in *OSt*-Tam3 also showed several single nucleotide polymorphisms (SNPs) (Supplementary Fig. 5B). Either this sequence rearrangement and/or SNPs found in *OSt*-Tam3 might be the cause of the suppression of Tam3 transposition associated with the *OSt*-Tam3 locus.

Isolation of *NSt*

NSt/*niv*$^{rec:\ beni}$ (HAM3) was derived from *nst*/*niv*$^{rec:\ beni}$ (HAM5) and was identified as a spontaneous mutant of *NSt* (Hashida et al., 2006; Uchiyama et al., 2008). *nst*/*niv*$^{rec:\ beni}$ shows red spots and sectors on the white background petal (> 1000 spots per flower) at 15℃ due to Tam3 transposition from the *niv*$^{rec:\ beni}$ allele (Uchiyama et al., 2013) (Fig. 2A). Both the lines share the *niv*$^{rec:\ beni}$ allele, whereas *NSt*/*niv*$^{rec:\ beni}$ shows no variegation (<10 spots per flower) at 15℃, indicating immobilization of Tam3 at the *niv*$^{rec:\ beni}$ locus (Fig. 2A). PCR detected the 2.0 kb Tam3 excision band from *niv*$^{rec:\ beni}$ in *nst*/*niv*$^{rec:\ beni}$ grown at 15℃, but not in *NSt/niv*$^{rec:\ beni}$ or the plants grown at 25℃, confirming that *NSt/niv*$^{rec:\ beni}$ carries the *NSt* locus that suppresses Tam3 transposition (Fig. 2A).

We crossed *NSt/niv*$^{rec:\ beni}$ (HAM3) × *nst/niv*$^{rec:\ beni}$ (HAM5) twice, independently (Supplementary Fig. 2B). A total of the 214 F_2 progenies of *NSt*/*niv*$^{rec:\ beni}$ × *nst*/*niv*$^{rec:\ beni}$ segregated into two different classes: high-spots (> 1000 spots per flower), and low-spots (<10 spot per flower) with a 1: 3 ratio of the number of plants (Supplementary Table 1 and Supplementary Fig. 2B). These results confirmed that excision of Tam3 from the *niv*$^{rec:\ beni}$ locus was controlled by a single dominant locus (*NSt*) as reported by Hashida *et al*. (2006).

By analogy to the method used for identification of *OSt*, we undertook transposon tagging using Tam3 as a probe to identify the Tam3-associated fragment specifically linked to the *NSt* phenotype. Detailed procedures for transposon tagging of *NSt* are described in Supplementary Description 2. We identified an *Eco*RV restriction enzyme DNA fragment linked to *NSt*, which was 3.5 kb long and contained 0.8 kb of

Tam3 sequences at the two ends of the *Eco*RV fragment with a 1.9 kb internal sequence (Supplementary Fig. 6). Further structural analysis of the sequence surrounding the 3.5 kb fragment in the *NSt*/*niv*$^{rec: beni}$ (HAM3) genome revealed two intact Tam3 sequences in head-to-head orientation inserted into the third intron of the *Am02g32060* gene encoding transcription factor BREVIS RADIX protein (Fig. 2B). Dot plot analysis of the sequence in this region showed that the two Tam3 sequences have the same structure as the reference element in the *niv*^{rec} allele (Hehl et al., 1991) (Supplementary Fig. 7A). In the *nst*/*niv*$^{rec: beni}$ (HAM5) genome, the right-hand copy of the two Tam3 sequences is absent (Supplementary Fig. 7B). Hence, the *NSt* locus of *NSt*/*niv*$^{rec: beni}$ (HAM3) may have arisen by *de novo* insertion of Tam3 on the right side of the Tam3 element in the *nst* allele of *nst*/*niv*$^{rec: beni}$ (HAM5) (Supplementary Fig. 7B). The *Am02g32060* gene residing *NSt* was found in the Snapdragon genome database to be located at the end of chromosome 2 (Fig. 2B and Supplementary Fig. 3).

Transcription, translation, nuclear import, and DNA-binding of Tam3 TPase

We then examined how the two *Stabiliser* loci inhibit Tam3 transposition. Tam3 transposition requires four steps involving the *Tam3 TPase* gene: transcription, translation, nuclear import, and binding to Tam3 elements. Regarding the transcription and translation of the *Tam3 TPase* gene, we performed qRT-PCR to detect differences in *Tam3 TPase* gene expression and immunoblot analysis to examine the translated product in the *OSt* (HAM21), *NSt* (HAM3), and *ost*/*nst* (HAM5) (Supplementary Description 3). The transcription and translation for the *Tam3 TPase* gene could not be quantitatively distinguished between *OSt*, *NSt*, and *ost*/*nst* plants (Supplementary Fig. 8; Supplementary Description 3). These results confirmed previous reports that *OSt* and *NSt* do not suppress the *Tam3 TPase* gene (Uchiyama et al., 2008).

We then examined the nuclear import of Tam3 TPase in the presence of *OSt* and *NSt*. When plants are grown at 15°C, Tam3 TPase is synthesized in the cytoplasm and enters the nucleus. We tested the nuclear import of Tam3 TPase by transient assay

using *Antirrhinum* protoplasts transformed with a construct for GFP-fused Tam3 TPase in the presence of *OSt* and *NSt.* We found that nuclear-localized GFP signals were observed more frequently in all protoplasts from *OSt*, *NSt*, or *ost*/*nst* plants at 15℃ compared to 25℃, indicating that nuclear import of Tam3 TPase at the low temperatures occurs in *OSt* and *NSt* genetic backgrounds, and confirming early reports that temperature and *OSt* influence Tam3 transposition independently (Fig. 3A and B; Supplementary Table 2) (Fincham and Harrison, 1967).

Following these experiments, we concluded that the two *Stabilisers* are probably involved in the final step of Tam3 transposition, the binding of Tam3 TPase to Tam3 DNA sequences, to limit Tam3 transposition. We therefore investigated the effect of *OSt* and *NSt* on the binding affinity of Tam3 TPase to its target sites. Electrophoretic mobility shift assay (EMSA) was performed using a 26 bp fragment containing three Tam3 TPase target motifs (GCHCG) as a probe (Hashida et al., 2006). Nuclear protein extracted from young leaves was employed to test the interaction between Tam3 TPase and the 26 bp target fragment. We confirmed that TPase protein extracted from all the plants grown at 15℃ was detected as probe-protein shift bands in nuclear fractions (Fig. 3C and D). Interestingly, strongly shifted bands were observed in the extracts from *OSt* plants grown at 15℃, which was consistent with the higher frequency of nuclear localized GFP signals in the protoplasts (Fig. 3B). However, neither *OSt* and *NSt* altered the binding affinity of Tam3 TPase to its target motifs.

mRNA profiles in *OSt* and *NSt*

According our results and those of others (Chatterjee and Martin, 1997), it was assumed that *OSt* and *NSt* interfere with the ability of the Tam3 TPase to bind to its target sequences on the chromosome, without compromising Tam3 TPase production. Firstly, we investigated whether the *OSt*- and *NSt*- factors might be RNA products, so we carried out poly(A)-enriched RNA-seq analysis to explore the transcription of the *Tam3 TPase* gene in mRNA from the *OSt*, *NSt*, and *ost*/*nst* plants. Similar transcriptional patterns of the sense strand of *Tam3 TPase* open reading frame (ORF)

were observed in these three genotypes, confirming the results of qRT-PCR and immunoblotting analyses (Supplementary Figs. 8-9). In *OSt* plants we found mRNA transcripts in the region of the pseudo-*Tam3 TPase* gene, although no transcripts were detected covering the 5' rearranged region of *OSt*-Tam3 (Supplementary Fig. 10). In *NSt* plants mRNA transcripts were observed for the internal region between two Tam3 elements in *NSt* locus, corresponding to transcripts from the third intron of the *Am02g32060* gene, but these aberrant transcripts did not align with the TPase transcript and therefore were unlikely to interact directly with the TPase (Supplementary Fig. 11). Although the two *Stabiliser* genes, *OSt* and *NSt*, gave rise to different mRNA expression patterns between the three genotypes, these different patterns of the RNA-seq data could not be related directly to the suppression of Tam3 transposition of *OSt* and *NSt*.

lncRNA profiles in *OSt* and *NSt*

The mRNA patterns in *OSt* and *NSt* did not show that high-expression poly(A)-tailed mRNAs were responsible for the suppression of Tam3 transposition. Thus, we investigated whether other RNAs, non-coding RNAs, might be derived from *OSt* and *NSt* loci and inhibit the binding of Tam3 TPase to Tam3 DNA sequences. One type of non-coding RNA is long non-coding RNA (lncRNA) the length of which is longer than 200 nucleotides and has important biological functions, including interacting with proteins to inhibit their binding to specific regions of DNA and interacting with DNA to decrease chromatin accessibility (Statello et al., 2021). Therefore, we performed rRNA-depleted RNA-seq analysis to investigate whether lncRNAs were generated from *OSt* and *NSt* loci. Within the Tam3 element, RNA transcripts (lncRNAs and mRNAs) were found in the *Tam3 TPase* gene in *OSt*, *NSt* and *ost*/*nst* plants (expression level: *OSt* > *NSt* = *ost*/*nst*), but no RNA transcripts were detected in both the terminal GCHCG-enriched regions of Tam3 (Supplementary Fig. 12). In *OSt*, we found RNA transcripts located in the pseudo-*Tam3 TPase* gene, although transcripts were missing for the 5' rearranged region of *OSt*-Tam3 (Supplementary Fig. 13). In the *NSt* locus, abundant RNA transcripts were detected in the inter-

element region between Tam3-L and -R in *NSt* plant, and a few transcripts existed in the same region in *ost*/*nst* plant (Supplementary Fig. 14). However, we were unable to infer any direct relationship between *NSt*-derived lncRNAs and Tam3 inactivation. Therefore, the results of different RNA expression patterns in the three plant lines could not be directly associated with the Tam3 silencing caused by either of the two *Stabiliser* loci.

sRNA profiles of Tam3 in *OSt* and *NSt*

Based on knowledge of sRNAs that play a role in transposon inactivation (Castel and Martienssen, 2013; Ito, 2013), we performed sRNA-seq analyses to investigate whether sRNAs are associated with Tam3 inactivation in either *OSt* or *NSt* plants. The functions of sRNAs are generally determined by their size: 21 nt and 22 nt for mRNA cleavage and 24 nt for DNA methylation (Kryovrysanaki et al., 2022). sRNAs from *OSt*, *NSt* and *ost/nst* plants were classified by function and compared between the three genotypes in terms of their distribution and abundance (Supplementary Figs. 15-16). 21-22 nt and 24 nt sRNAs on sense and antisense strands of the Tam3 sequence accumulated more from *NSt* genotypes and the two genotypes, respectively. sRNAs were detected mainly in the coding region of the TPase (690 - 3101 bp of the Tam3 element), the distribution patterns of which were more or less similar between the three genotypes (Supplementary Figs. 15-16). We found no clear difference in either the accumulation or distribution patterns of sRNAs between the three genotypes. However, despite the accumulation of sRNAs in the 5' terminal region of the Tam3 element being low, the distribution patterns were different between the three genotypes (Supplementary Figs. 15-16). We focused our investigations on the sRNAs from the 5' terminal regions where Tam3 TPase binding motifs are present.

sRNAs from the x and y regions of the 5' terminus of Tam3 could be associated with the *Stabiliser* properties (Fig. 4), while, in contrast, the accumulations of sRNAs were detected only weakly in the 3' terminus of the three genotypes (Supplementary Fig. 17). The three genotypes differentially accumulated sRNAs from the sense strand of

the x and y regions of Tam3 (Fig. 4), suggesting that these sRNAs may bind to the antisense strand. In *OSt* plants, sRNAs from the first 30 bp region of the 5' terminus of Tam3, which contains the terminal inverted repeat (TIR) sequence and a GCHCG motif on the antisense strand, strongly accumulated (Fig. 4). These sRNAs were almost from those with a single SNP on the 13th nucleotide position from the 5' end of the x' and x'' segments in *OSt*-Tam3 (Supplementary Figs. 5B and 18). In *NSt* plants, sRNAs from the sense strand of the specific 70-150 bp region accumulated strongly and might protect binding to the x segment containing four TPase GCHCG binding motifs corresponding to the antisense sequence, and also sRNAs accumulated in the first 30 bp region at a relatively high level (Fig. 4). Compared with *OSt* and *NSt*, sRNAs from *ost*/*nst* plants were observed at a quite low detectable levels from the sense strand of the first 30 bp region (Fig. 4). For the antisense strands, a relatively low accumulation of sRNA from *OSt* and *NSt* was observed for the 30-70 bp region of the x segment which includes six GCHCG motifs corresponding to the sense strand sequence (Fig. 4).

sRNA profiles in *OSt* and *NSt* sequences

Based on the previous sRNA-seq results, we observed that specific sRNAs accumulated in the 5' region of Tam3 sequence in *OSt* and *NSt* lines, compared to the *ost*/*nst* line (Fig. 4; Supplementary Figs. 15-16). In both the sense and antisense strands of the *OSt* sequence, most of the sRNAs were distributed in the region from the 5' end of *OSt*-Tam3 to the end of the pseudo-*Tam3 TPase* gene (1-3385 bp of the *OSt*-Tam3 sequence) (Supplementary Fig. 18). In the 5' end of the *OSt*-Tam3 sequence, 24 nt sRNAs came predominantly from the x', x'' and z'' regions on the sense strand and from the z'' region on the antisense strand (Supplementary Figs. 18 and 19A-B). We could detect sRNAs specifically from the antisense strand of the 5' end of Tam3-L in the *NSt* allele, which was not the case for the *nst* allele (Supplementary Fig. 19C-D).

In general, double-stranded RNAs produced by pairing sense and antisense transcripts

of DNA fragments and transcribing inverted repeats can be processed into sRNAs (Mathieu and Bender, 2004). The production of sRNAs on *OSt* and *NSt* sequences is most likely due to the bidirectional transcription of *OSt*-Tam3 and the transcription of two inverted Tam3 elements for *NSt*, respectively. We performed a promoter prediction on the 6675 bp surrounding the *OSt*-Tam3 sequence and the 9133 bp surrounding the *NSt* elements and mined for possible transcription start sites (TSSs) on the sense and antisense strands of the two sequences (Supplementary Table 3). According to the TSS score, 32 sites on the sense and antisense strands of *OSt* and 46 sites on the sense and antisense strands of *NSt* were identified (Supplementary Table 3). Based on the distribution of the sRNAs and TSS scores in the *OSt*-Tam3, two TSS combinations were identified in the flanking and inside sequences (Fig. 5A). In *NSt*, since no antisense RNA was detected from the internal sequence between the two Tam3 elements (Supplementary Figs. 11 and 14), it is likely that only sense strand transcription occurred from the Tam3 on the left to the Tam3 on the right-hand side. This transcript could result in a hairpin structure with both Tam3 5' sequences, giving rise to the specific sRNAs observed (Fig. 5B). Transcription from *OSt* and *NSt* could generate sense-antisense paired and hairpin (stem-loop) dsRNAs, respectively (Fig. 5). The predicted promoter activities on *OSt* and *NSt* alleles suggested that their respective transcription might generate sRNAs as Tam3-specific repressors.

Detection of hairpin transcript in *NSt*

According to our finding of sense transcripts in the internal region between two Tam3 of *NSt*, it is most likely that the transcription of *NSt* from Tam3-L to Tam3-R could result in a hairpin structure which lie in head-to-head orientation. This hairpin transcript could be processed into the specific sRNAs. To examine for presence of the hairpin transcript, PCR analyses were performed for the stem and loop parts of the hairpin product using two pairs of primers, respectively (Supplementary Fig. 20). The two parts only can be detected in *NSt* hairpin transcript together (Supplementary Fig. 20). We were unable to amplify cDNAs beyond both Tam3 sequences, which may be because DNA polymerase was unable to extend to the double-stranded stem region of

a stem-loop structure from the single-stranded loop (Zhong et al., 2019). The results suggested that transcription of *NSt* can result in a hairpin transcript with the 5' end regions of Tam3 then responsible for the generation of the specific sRNAs.

Induction of sRNA by TRV-mediated virus-induced gene silencing (VIGS)

Based on the previous results of sRNA-seq analyses and the detection of *NSt* hairpin transcript, *OSt*- and *NSt*-derived sRNAs located in the 5' terminal Tam3 region might most likely cause Tam3 transposition suppression. Tan *et al*. (2020) reported that VIGS-mediated sRNA induction is available in *Antirrhinum*. Thus, to confirm the hypothesis, we performed TRV-mediated VIGS in *ost*/*nst* plants to induce sRNAs transcribed from 5' terminal Tam3 fragment, and then we observed whether the sRNAs can have suppressive effect on Tam3 transposition following the inoculated *ost*/*nst* plants grown at 15 ℃. When the *ost*/*nst* plants with or without TRV-Tam3 inoculation were grown at low temperatures, the variegation phenotype on the leaves of inoculated plants strongly decreased compared with that in Mock-inoculated and no-inoculated plants (Fig. 6A). RT-PCR analyses were carried out to identify the transcript derived from *CP* gene to inserted Tam3 fragment (Fig. 6B). We observed ~700 bp band for *CP*-Tam3 transcripts in the *ost*/*nst* plants to confirm the successful inoculation of TRV-Tam3 (Fig. 6B). To detect sRNAs induction in *ost*/*nst* plants with TRV-Tam3 or mock inoculation, we performed sRNA-seq analyses. The accumulations of total sRNAs (21, 22, 23 and 24 nt) in the 242 bp 5' terminal region of Tam3 sequence, inserted into TRV RNA2 vector, were compared between TRV-Tam3- and mock-inoculated *ost*/*nst* plants. As shown in Fig. 6C, the accumulation of Tam3-derived sRNAs was higher in TRV-Tam3 plants than that in the mock plant, which indicated that Tam3-derived sRNAs were induced in TRV-Tam3 plants. Eight loci with single Tam3 insertion were capable of excising Tam3 in HAM5 line, and two of the loci, *niv*^{rec} and *S78*, was highly active (Kitamura et al., 2001). Thus, we performed PCR analyses to estimate Tam3 excision rate at the two loci. In the TRV-Tam3 inoculated plants, their excision bands were weaker than that in mock-inoculated and no-inoculated plants (Supplementary Fig. 21). To accurately assess

Tam3 excision rate, we analyzed the intensity of the excision bands obtained by PCR. We found that Tam3 transposition rates at the two loci were significantly lower in TRV-Tam3 inoculated plants than that in controlled plants (Fig. 6D). These results suggested that sRNAs originated from 5' terminal Tam3 region suppressed the Tam3 transposition in the *ost*/*nst* plants.

Discussion

Although the two *Stabiliser* loci have distinctive structures and chromosomal positions, both play suppressive roles in Tam3 transposition. The *OSt* locus, carrying the pseudo-Tam3 lies in an intergenic region on chromosome 5 of the *OSt*/*niv*^{rec} (HAM21) line. The unique feature of the *OSt* locus is that its causative rearrangement occurred in the terminal region of the element, outside of the *TPase* coding sequence. The *NSt* locus on chromosome 2 involves two Tam3 fragments inserted in head-to-head orientation in the third intron of the *Am02g32060* gene in the *NSt*/*niv*$^{rec: beni}$ (HAM3) line.

Currently, four TE-specific repressor genes have been identified such as *En-I102* for En/Spm in maize, *Muk* for Mu element in maize, and *KP* and *Lk-P(1A)* for P element in *Drosophila* (Black et al., 1987; Cuypers et al., 1988; Ronsseray et al., 1991; Slotkin et al., 2003). *En-I102* and *KP* are the deletion derivatives of En and P elements, respectively (Black et al., 1987; Cuypers et al., 1988). *Lk-P(1A)* and *Muk* share the head-to-head structure of their respective TEs (Roche and Rio, 1998; Slotkin et al., 2005). *Lk-P(1A)* has two intact P elements, whereas *Muk* was generated by duplication of partially deleted *MuDR* element (Ronsseray et al., 1996; Roche and Rio, 1998; Slotkin et al., 2005).

Based on the mechanisms of suppression, the four examples of DNA transposable element suppression can be divided into two groups: pre-translational suppression and post-translational suppression. The pre-translational repression group includes *Muk*

and *Lk-P(1A)*, which generate small interference RNAs (siRNAs) for the degradation of *TPase* transcripts (Slotkin et al., 2005; Brennecke et al., 2008; Majumdar and Rio, 2015). These TE-specific repressor genes have a rearranged segment of the authentic TE structure, which could lead to siRNAs against the *TPase* gene transcript (Slotkin et al., 2005; Brennecke et al., 2008; Majumdar and Rio, 2015). The other two examples, *En-I102* and *KP*, involve post-translational suppression (Cuypers et al., 1988; Lee et al., 1998). Both *En-I102* and *KP* can produce aberrant TPase to compete with normal TPase for target sites on TEs (Cuypers et al., 1988; Lee et al., 1998).

OSt and *NSt* belong to a third group, with mechanisms distinct from pre-translational suppression or post-translational repression. These *Stabiliser* genes do not restrict transcription and translation of the *TPase* gene like *Muk* and *Lk-P*(*1A*), nor do they generate aberrant truncated TPase to compete for target sites at the termini of the element, like *En-I102* and *KP*. All these results suggest that the mechanism(s) of repression by *OSt* and *NSt* on Tam3 transposition are distinct from the general epigenetic regulation of TEs (Wang et al., 2022).

The *OSt* and *NSt* lines retain the ability of the Tam3 TPase to recognize and bind the Tam3 sequence because EMSA showed the ability of nuclear Tam3 TPase to bind to the 26 bp DNA sequence containing three GCHCG motifs (Fig. 3C-D). Thus, it is most likely that both *OSt* and *NSt* alter the recognition by the Tam3 TPase of its binding motifs. In general, DNA methylation and histone modification could create barriers on the DNA sequence to prevent recognition and binding of DNA-binding proteins, resulting in transcriptional inhibition (Slotkin and Martienssen, 2007; Miller and Grant, 2013; Liyanage et al., 2014). However, our results do not support the involvement of DNA methylation or histone modification, as the transcription of *Tam3 TPase* occurs normally (Supplementary Fig. 8). Consequently, there are two possible ways that entities derived from the *OSt* and *NSt* loci restrict the binding of Tam3 TPase to Tam3 sequences (Fig. 7). One is that the recognition sites of Tam3 TPase are covered by such entities (Fig. 7A), and the other is that such entities

compete for Tam3 TPase preventing it from binding (Fig. 7B). In this study, we found that sRNAs from the x and y regions of the Tam3 5’ terminal sequence exist in *OSt* and *NSt* lines (Fig. 4). The sRNAs were induced into *ost/nst* plants by TRV-mediated VIGS, and the suppression of Tam3 transposition was confirmed in TRV-Tam3-inoculated *ost*/*nst* plants (Fig. 6). Thus, these sRNAs might compete with the Tam3 TPase for the GCHCG motifs or interact with Tam3 TPase itself, and thus the prevent the TPase from binding, resulting in the suppression of Tam3 transposition (Fig. 7). For the above reasons, the function of these sRNAs is likely different from known TEs-derived sRNAs (Okamoto and Hirochika, 2001).

OSt and *NSt* could generate sRNAs that cover the target sites of Tam3 TPase (Fig. 7A) or that interact with Tam3 TPase (Fig. 7B) so that Tam3 transposition is suppressed. In the 5’ end region of the Tam3 sequence, we observed that the sRNA accumulations in the *OSt* and *NSt* lines are clearly different from those in the *ost*/*nst* line (Fig. 4). In the sense strand, there are six GCHCG motifs in the region where more sRNAs were observed in *OSt* and *NSt* relative to *ost*/*nst* (Fig. 4). Notably, the sRNA accumulation was observed on the sense strand opposite the GCHCG motif on the antisense strand. The sRNAs accumulate in the common 5’ end region of Tam3 in the two lines suggesting that *OSt* and *NSt* suppress Tam3 transposition by similar mechanisms. However, *OSt* and *NSt* differ in the localizations of their sRNAs and in the sRNA types from the sense strand of the 5’ end of Tam3 where the Tam3 TPase binds (Fig. 4 and Supplementary Figs. 15-16). In plants, sRNAs are commonly generated from dsRNAs derived from hairpin RNAs or pairing of sense and antisense RNAs by cleavage by dicer proteins (Mathieu and Bender, 2004; Ciechanowska et al., 2021; Kryovrysanaki et al., 2022). The TSSs in *OSt* and *NSt* were generated by spontaneous structural variation. The sRNA of *OSt* is derived from the rearrangement of the 5' end sequence of Tam3 and the sequence of the neighboring sequence (Fig. 5A). The possibility that the rearrangement of the 5' end sequence of Tam3 in *OSt* generated a *de novo* TSS is supported by the fact that antisense transcripts of normal Tam3 were rarely detected in mRNA and lncRNA (Supplementary Figs. 9, 10, 12, 13). *NSt* could

be a hairpin loop formed by the extension of a one-way transcription product of the sense strand from Tam3-L to Tam3-R. This possibility is suggested by the transcription pattern of mRNA and lncRNA in the *NSt* region (Fig. 5B, Supplementary Fig. 11, 14). The 5' end region of Tam3 contains a TSS that is transcribed in the antisense direction, but it is not clear why transcription occurs only in the sense direction of Tam3-L but not Tam3-R. It may be related to the fact that the direction of transcription is the same as that of the inserted host gene.

The sRNA types preferentially detected in the *OSt* and *NSt* lines were 24 nt and 21-22 nt sRNAs, respectively. These differences could indicate that different dicer proteins function predominantly in the two lines (Supplementary Figs. 15-16). The dicer proteins are known as DICER-LIKE (DCL), and include at least DCL1, 2, 3 and 4 (Kryovrysanaki et al., 2022). Four DCL proteins are responsible for the generation of different sized sRNAs: DCL1 and 4 for 21 nt sRNAs, DCL2 for 22 nt sRNAs and DCL3 for 24 nt sRNAs (Erdmann and Picard, 2020; Kryovrysanaki et al., 2022). Normally, 24 nt sRNAs are associated with transcriptional gene silencing, whereas 21 and 22 nt sRNAs are involved in post-transcriptional gene silencing (Erdmann and Picard, 2020; Kryovrysanaki et al., 2022). It may be that different DCL proteins led to distinct sRNAs in the *NSt* and *OSt* lines, associated with their different respective precursors: double-stranded duplex in *OSt* and single RNA molecule with hairpin shape in *NSt* (Fig. 5). These results are clearly consistent with most 24 nt sRNAs in *OSt* being generated from double-stranded duplexes by DCL3, and the 21-22 nt sRNAs in *NSt* being derived from the double-stranded stem region of a hairpin-shaped RNA by DCL1 and 2 (Liu et al., 2014). These different mechanisms forming different sRNAs in *OSt* and *NSt* could be associated with semi-dominant and dominant suppressive effects of *OSt* and *NSt* respectively on Tam3 transposition, implying that the suppression by *NSt* involving the hairpin and DCL1 & 2 activity is stronger than that invoked by *OSt.* In 5’ region of Tam3, the distribution of sRNAs covering the targeting area of Tam3 TPase was wider in *NSt* than that in *OSt* (Fig. 4 and Supplementary Figs. 15-16). The distinct distribution range of sRNAs might suggest

that Tam3 transposition is suppressed by *OSt* and *NSt* at semi-dominant and dominant levels, respectively.

Most TEs are inactive and are tightly regulated by hosts via master regulators, which maintain the integrity and stability of host genomes (Levin and Moran, 2011; Bhat et al., 2022). In particular, master regulators prevent large-scale TE transpositions. However, a very small proportion of TEs are active and continue to transpose under repressive conditions (Slotkin and Martienssen, 2007). The transposition of these active TEs may be regulated by more specialized mechanisms. Our work shows that TE-specific repressor genes may involve spontaneous changes that arise as a result of transposition of active TEs, resulting in self-regulation. TE-specific repressor genes can be found and detected for DNA TEs whose transposition activity can be monitored easily. Although six TE-specific repressor loci, including *OSt* and *NSt*, have now been isolated and characterized in different organisms, these loci may arise only by chance. Such self-regulatory systems could provide a means for active TEs to maintain a balanced relationship with their hosts when they escape from master regulation. Within TE self-regulatory systems, TE-specific repressor loci could be a characteristic of active TEs, at least class II, DNA TEs.

Materials and Methods

Plant Materials

Four lines of *Antirrhinum majus* were used in this study, two Tam3-active and two Tam3-repressed lines (Supplementary Fig. 2). One of the Tam3-active lines derived from the John Innes Center (JIC) stock JI: 98, here named HAM2, has the genotype for *ost*/*nst*/*niv*^{rec}/*Pal* (Supplementary Fig. 2A). The other Tam3-active line called HAM5 contains the genotype for *ost*/*nst*/*niv*$^{rec:\ beni}$/*Pal* (Supplementary Fig. 2B). This line was isolated from the progeny of JI: 98 (H101) carrying the *niv*^{rec} allele crossed with the two different lines: Stock 44 and 45 in the JIC collections (Uchiyama et al., 2013). In the two Tam3-repressed lines: the JIC stock JI: 558 carrying *OSt* had been

produced by crossing *niv*^{rec}:98 to the original *Stabiliser* line, stock JI: 3 (*OSt*/*nst*/*Niv*/*pal*^{rec}) (Harrison and Carpenter, 1973), and the *OSt*/*nst*/*niv*^{rec}/*Pal* genotype had been selected, here named HAM21. The other *St* line, called HAM3, carrying *ost*/*NSt*/*niv*$^{rec:\ beni}$/*Pal*, which is an isogenic line of HAM5 (o*st*/*nst*/*niv*$^{rec:\ beni}$/*Pal*) (Uchiyama et al., 2008). To supplement the *OSt*/*niv*^{rec} (HAM21) and *ost*/*niv*^{rec} (HAM2) test cross, we also crossed JIC Stock2 (*ost*/*nst*/*Niv*/*pal*^{rec}) named HAM22, to HAM21 and examined the segregation of the petal variegation trait in the F_2 population. To obtain F_2 seeds, we made three combinations of crosses [*ost*/*niv*^{rec} (HAM2) × *OSt*/*niv*^{rec} (HAM21)], [*ost*/*Niv*/*pal*^{rec} (HAM22) × *OSt*/*niv*^{rec}/*Pal* (HAM21)], and [*nst*/*niv*$^{rec:\ beni}$ (HAM5) × *NSt*/*niv*$^{rec:\ beni}$ (HAM3)]. Plants were initially grown at 25℃ for 1.5 months and transferred to 15℃ or 25℃ growth chambers and grown for at least 2 weeks to score their petal variegation phenotypes.

Additionally, Tobacco cv. Xanthi was also used in the study. The Tabacco seeds were sterilized with ethanol and bleach, and sowed on 1/2 Murashige and Skoog agar media. Following germination at 21 ℃ for 1 week, Tabacco seedlings were transplanted individually into soil pots for subsequent growth at 21 ℃.

DNA extraction and PCR analysis

DNA was extracted from young leaves (3-4 cm in length) of *Antirrhinum* plants using extraction buffer (100 mM Tris-HCl [pH 8.0], 10 mM EDTA [pH 8.0], 1 M KCl) combined with phenol/chloroform extraction method. PCR analysis was performed using genomic DNA. The PCR solution containing 200 ng of DNA and components of Ex Taq DNA polymerase (Takara Bio, Shiga Japan) was denatured at 94 ℃ for 30 s, annealed at appropriate temperatures based on the melting temperature for each primer for 30 s, and extended at 72 ℃ for a given time based on the length of the amplified fragments for a total of 30 cycles. Each primer set used for PCR was listed in Supplementary Table 4.

Phenotypic segregations in the F_2 populations and transposon tagging

Based on flower variegation phenotypes at the *Niv* locus, phenotypic segregations were investigated using F_2 plants obtained by selfing F_1 plants from crosses between the highly variegated lines [*ost*/*niv*^{rec} (HAM2) or *nst*/*niv*$^{rec: beni}$ (HAM5)] and the *Stabiliser* lines *NSt*/*niv*$^{rec: beni}$ (HAM3) or *OSt*/*niv*^{rec} (HAM21). The F_2 plants between *ost*/*niv*^{rec} (HAM2) and *OSt*/*niv*^{rec} (HAM21) were sorted into high- (>2500 spots per flower likely *ost*/*ost; niv*^{rec}/*niv*^{rec}), middle- (100-500 spots per flower likely *OSt*/*ost; niv*^{rec}/*niv*^{rec}) and low- (<20 spots per flower likely *OSt*/*OSt; niv*^{rec}/*niv*^{rec}) spotted plants and were used for transposon tagging (Supplementary Fig. 2A) (Martin et al., 1985). For *NSt*, F_2 plants between *nst*/*niv*$^{rec: beni}$ (HAM5) and *NSt*/*niv*$^{rec: beni}$ (HAM3) were segregated into high spot (> 1000 spots per flower likely *nst*/*nst; niv*$^{rec: beni}$/*niv*$^{rec: beni}$) and low spot (<10 spots per flower, likely *NSt*/*NSt; niv*$^{rec: beni}$/*niv*$^{rec: beni}$ and *NSt*/*nst; niv*$^{rec: beni}$/*niv*$^{rec: beni}$) (Supplementary Fig. 2B).

A possible reason for the *Stabiliser* phenotypes has long been proposed to be related to alterations in Tam3 itself (Fincham and Harrison, 1967). To investigate the relationship between Tam3 and petal variegation phenotypes, Southern hybridizations were performed for both F_2 segregations in the *OSt* and *NSt* populations using the Tam3 sequence as a probe (Kishima et al., 1999). For Southern hybridizations, *Eco*RI- and *Eco*RV-digested genomic DNAs for the *OSt* and *NSt* populations, respectively, were transferred to Hybond-N+ membranes (Pall, http://www.pall.com); all procedures were performed using an ECL Direct Nucleic Acid Labeling and Detection System in accordance with the manufacturer's instructions (GE Healthcare, http://www.gelifesciences.co). In the Southern hybridization pattern of the *OSt* F_2 population using the Tam3 sequence as a probe, we found the 6.6 kb-Tam3 *Eco*RI fragment linked to the *St* phenotypes (Supplementary Fig. 4A), while the hybridization pattern in the *NSt* F_2 population showed 3.5 kb-Tam3 *Eco*RV fragment linked to the *St* phenotypes (Supplementary Fig. 6A). The bands were purified from agarose gels at the appropriate sizes in accordance with Martin et al. (1985). The procedures of Tam3 transposon tagging for *OSt* and *NSt* are detailed in Supplementary Description 1 and 2.

The association with the *OSt*/*ost* phenotypes was validated for 64 individuals by two PCR amplifications: one primer combination of R [ATA AAC CCT AAC GAA CGA GGT GGA AAT G] and F1 [GAA CCC CAC TCG AAG ACG GAT TG] amplified the sequence without the *OSt*-Tam3 insertion for the *ost* allele (3.0 kb), and the other primer combination of R and F2 [CCA ACA ATC CAA CCA ACC AAG] resulted in amplification of the sequence with the *OSt*-Tam3 insertion for the *OSt* allele (1.5 kb) (Supplementary Fig. 4C; Supplementary Table 4). The linkage of the *NSt* locus with the tagged sequence was examined and confirmed for more than 200 individuals by PCR with two primer combinations: one primer combination of F1 [AAG GCT TTC ATT GCA TAG GGA TCT GG] and R1 [CCA AGT ACT GAA TAA GCA GGA GGT GAA] amplified the sequence without the Tam3-R insertion for *nst* allele (0.7 kb), and the other combination of F2 [GAA CCG GCT GGA GAA ATG] and R2 [AGC TGC AGC ACA AAA AAC AGG CCT ATA C] gave rise to the amplification of the sequence with Tam3-R insertion for *NSt* allele (0.33 kb), and Southern hybridization with the probe of the flanking sequence to Tam3 in the selected clone (Supplementary Fig. 6C and D; Supplementary Table 4). The chromosomal positions for the *OSt* and *NSt* loci were determined with Snapdragon Genome Database at http://bioinfo.sibs.ac.cn/Am/index.php.

RNA extraction and qRT-PCR

Total RNA was extracted from young leaves of *Antirrhinum* plants using PureLink® RNA Mini Kit (Thermo Fisher Scientific). Approximately 800 ng of total RNA was reverse transcribed into cDNA using QuantiTect Reverse Transcription Kit (QIAGEN) according to the manufacturer's instructions. qRT-PCR was performed to detect the expression level of *Tam3 TPase* gene on CFX Connect™ Real-Time System (BIO-RAD) using SYBR® GreenER™ qPCR SuperMix (Thermo Fisher Scientific). The *Antirrhinum UBIQ* gene was used as internal control. Primers used for qRT-PCR are listed in Supplementary Table 4.

Total protein extraction

The leaf powder of *Antirrhinum* plant material was mixed with the protein extraction buffer (50 mM Tris-HCl [pH 7.5], 150 mM NaCl, 1 mM EDTA, 10% glycerol, 5 mM DTT, 0.2% TritonX-100, and protease inhibitor cocktail [Sigma-Aldrich]), and the homogenate was incubated on ice for 30 min with shaking. After incubation, the homogenate was centrifuged at 13,000 rpm for 15 min at 4 ℃. The supernatant was collected and centrifuged at 13,000 rpm for 10 min at 4 ℃, and the resulting supernatant was collected as total protein. The protein concentration was determined using a protein assay kit (Bio-Rad) before use.

Nuclear and cytoplastic proteins extraction

At least 1.0 g of *Antirrhinum* plant leaf powder was thoroughly mixed with Honda buffer (0.44 M sucrose, 20 mM HEPES-KOH [pH 7.4], 10 mM $MgCl_2$, 1 mM DTT, 1.25% Ficoll, 2.5% dextran T40, 0.5% TritonX-100, and protease inhibitor cocktail [Sigma-Aldrich]), and the homogenate was filtered through two layers of Miracloth (Sigma-Aldrich). The filtered homogenate was centrifuged at 3,500 rpm for 5 min at 4 ℃. After centrifugation, the supernatant was transferred into new tube and centrifuged at 14, 000 rpm for 10 min at 4 ℃, and then the new supernatant was collected as cytoplastic protein. The remained nuclear pellet was resuspended in Honda buffer and centrifuged at 3,500 rpm for 5 min at 4℃. The washing step was repeated for three times, and the final white nuclear pellet was resuspended in protein extraction buffer (50 mM Tris-HCl [pH 7.5], 150 mM NaCl, 1 mM EDTA, 10% glycerol, 5 mM DTT, 0.2% TritonX-100, and protease inhibitor cocktail [Sigma-Aldrich]). The nuclear mixture was incubated on ice for 30 min with shaking, then centrifuged at 13, 000 rpm for 20 min at 4℃. After centrifugation, the supernatant was collected as nuclear protein. The protein concentration was determined using a protein assay kit (Bio-Rad) before use.

Western blot analysis

Protein extracts were mixed with 5× protein loading buffer and denatured at 100 ℃ for 10 min. Denatured protein was separated on 10% SDS-PAGE gel and transferred to a polyvinylidene fluoride (PVDF) membrane. After blocking with 5% (w/v) skim milk at 4 ℃ overnight, the membrane was incubated with primary antibods: anti-RHL TAK HKN RDM DA rabbit serum (amino acid positions of immunogen oligopeptide is 220-223 in Tam3 TPase, produced by Eurofins Genomics K. K.) recognizing Tam3 TPase or Anti-dimethyl-Histone H3 (Lys4) rabbit serum (upstate) targeting demethylated Histone H3 (Lys4), for 1 hour at room temperature. The membrane was incubated with 5000-fold diluted secondary antibody (goat anti-rabbit IgG [H+L] horseradish peroxidase conjugate, BIO-RAD) for 1 hour at room temperature and stained with ECL detection reagents (GE Healthcare) according to the manufacturer's instructions. Signals were detected using a Fujifilm LAS4000mini Luminescence Imaging Analyzer.

Transient transformation of protoplast and microscopic observation

Protoplasts were isolated from young *Antirrhinum* leaves and transiently transformed with approximately 15 ug of pA7-Tam3 TPase-GFP plasmid DNA, used in Zhou *et al*. (2017), using PEG-calcium transfection method according to Yoo *et al*. (2007). After transient transformation, all samples were cultured at 25℃ for 20 h. Upon completion of culture, fluorescence signals were observed using an all-in-one fluorescence microscope (BZ-X810, Keyence).

EMSA

Nuclear protein was extracted as described above. The DNA probe used in Hashida *et al*. (2006) contained three Tam3 TPase binding motifs (GCHCG), and its nucleotide position is from 79 to 104 in the Tam3 sequence (see in Fig. 3D). To synthesize the DNA probe, the biotin-labelled positive-strand oligonucleotide was equally mixed with the negative-strand oligonucleotide, and the oligonucleotide mixture was incubated at 95℃ for 10 min and cooled down to produce the DNA probe. EMSA was

689 performed using the LightShift® chemiluminescent EMSA kit according to the
690 manufacturer's instructions.
691
692 **RNA-seq analyses**
693 Total RNA was extracted as described above. gDNA was removed from RNA using
694 Dnase I (Nippon Gene). RNA library preparation and sequencing were performed by
695 Rhelixa (Japan), and 150 bp paired-end (PE150) reads were generated.
696
697 For data analysis, raw sequences were processed to remove adapters and low quality
698 sequences using Trimmomatic (Bolger et al., 2014). Quality control of trimmed reads
699 was performed using FASTQC
700 (https://www.bioinformatics.babraham.ac.uk/projects/fastqc/). The trimmed reads
701 were then aligned to reference sequences using hisat2
702 (http://daehwankimlab.github.io/hisat2/). Aligned SAM files were converted to BAM
703 files using Samtools (https://www.htslib.org/), then read counts were performed on
704 BAM files using Samtools as well.
705
706 **sRNA-seq analyses**
707 Total RNA was extracted as described above. gDNA was removed from RNA using
708 Dnase I (Nippon Gene). sRNA library preparation and sequencing were performed by
709 Rhelixa (Japan).
710
711 For the data analysis, raw reads were processed to remove adapters and low-quality
712 reads using Trimmomatic (Bolger et al., 2014). In trimmed reads, reads that contain ≥
713 20 A or whose length is < 15 nt or >35 nt were removed using cutadapt
714 (https://cutadapt.readthedocs.io/en/stable/). After read cutting, quality control of the
715 reads was carried out using FASTAQC
716 (https://www.bioinformatics.babraham.ac.uk/projects/fastqc/). Then, rRNAs, tRNAs,
717 snRNAs, snoRNAs and known miRNAs were removed from qualified reads using

718 Rfam (https://rfam.org/) and miRbase (https://mirbase.org/) databases. The processed
719 reads were aligned to reference sequences using bowtie2 (https://bowtie-
720 bio.sourceforge.net/bowtie2/index.shtml). Aligned SAM files were converted to BAM
721 files using Samtools (https://www.htslib.org/). The screening of perfectly aligned
722 reads and three sized sRNAs (21, 22 and 24 nt), and read counting were carried out
723 with BAM files using Samtools.
724
725 **Plasmid construction**
726 The 242 bp of 5' terminal Tam3 fragment was amplified from *ost*/*nst* genome DNA by
727 PCR KOD FX Neo DNA polymerase (TOYOBO, Supplementary Fig. 22A). The
728 amplified fragment was cloned into T-Vector pMD20 using a ligation mix (Takara
729 Bio) following the manufacturer's instructions. Following the verification by Sanger
730 sequencing, the target fragment was cut and inserted into the BamHI and KpnI
731 restriction sites of the TRV RNA2 vector (pYL156, Addgene; Supplementary Fig.
732 22A). The primers used were listed in Supplementary Table 4.
733
734 **Virus-induced gene silencing (VIGS) assay in *Antirrhinum***
735 The TRV1 plasmid (pYL192, Addgene) and recombinant TRV RNA2 plasmids were
736 transferred into *Rhizobium radiobactor* (*R. radiobactor*, formerly *Agrobacterium*
737 *Tumefaciens*) GV3101 by freeze-thaw transformation. Transformed single *R.*
738 *radiobactor* clone was selected by culturing for two days at 28 ℃ on LB agar media
739 containing 50 ug/ml kanamycin and 20 ug/ml sodium rifampicin. Selected single
740 clone was grown in LB liquid containing the same concentrations of antibiotics
741 overnight with shaking (120-180 rpm). And 200 ul of the overnight cultured *R.*
742 *radiobactor* liquid was used to inoculate 100 ml LB liquid with antibiotics. Following
743 ~24 h culture, the cell concentration was measured by spectrophotometer (Hitachi U-
744 2810), and the OD_{600} of cell concentration was ~0.4. And then cells were pelleted by
745 centrifuging at 4,500 rpm for 2 min at room temperature and resuspended in freshly
746 prepared infiltration medium (10 mM MES pH 5.6, 10 mM $MgCl_2$, 150 uM

acetosyringone) to a final OD_{600} of 1.5 and incubated at dark, room temperature environment for 3 h. Cells carrying TRV1 were mixed with cells carrying TRV RNA2 or TRV RNA2 inserted with Tam3 fragment in a 1:1 volume ratio. The mixture was used to infiltrate leaves of 3 weeks-old Tobacco cv. Xanthi plants by needle-less syringe method. After 5-7 days, leaves higher on the plants showing symptoms of infection (distorted shape) were ground in phosphate buffer (0.577 mM Na_2HPO_4, 0.423 mM NaH_2PO_4, pH 7.0) on ice. 21 days-old *Antirrhinum* seedlings were inoculated by scattering carborundum over leaves, and the viral sap (10 ul per each organ) was pipetted on the leaves. Rubbing was performed between gloved finger and thumb until chlorophyll was seen to bleed into the buffer. Plants were then covered with transparent plastic lids for 3 days at high temperature to maintain a high relative humidity. After the pre-cultivation, the plants were transferred into 15 ℃ growth chamber to grow for at least two weeks.

Data depositions

The genomic sequences of the regions including *OSt* and *NSt* were deposited in NCBI GenBank PP898194 and PP898195, respectively. The RNA sequencing data for mRNA, long non-coding RNA (lncRNA), and small RNA (sRNA) were registered in NCBI Sequence Read Archive SAMN41273101 (HAM3 mRNA), SAMN41273102 (HAM21 mRNA), SAMN41273103 (HAM5 mRNA), SAMN41273104 (HAM3 lncRNA), SAMN41273105 (HAM21 lncRNA), SAMN41273106 (HAM5 lncRNA), SAMN41273107 (HAM3 sRNA), SAMN41273108 (HAM21 sRNA), and SAMN41273109 (HAM5 sRNA).

Acknowledgements

We gratefully acknowledge Dr. Y. Koide (Hokkaido University) for his valuable suggestions and comments. We also thank H. Zhou, M. Xu, S. Mitsui, H. Asano, and

R. Tanabe (Hokkaido University) for technical assistances. Seeds were kindly supplied by R. M. Carpenter and L. Copsey (John Innes Centre). This work was supported by JSPS KAKENHI grant #08760002.

Author contributions

C. M. and Y.K. made the initial concept of the study. W.S., T.U., and Y.K. designed the experimental plan. W.S., C.M., and Y.K. drafted the manuscript with input from all other authors. Y.K., T.U. and H.K. performed the transposon tagging. S.W., M.H., and I.Y. analyzed and evaluated genetic traits and phenotypes. S.W. and K.N. performed immunoblotting analyses and EMSA. S.W. performed most of the other molecular analyses.

References

Bhat A, Ghatage T, Bhan S, Lahane GP, Dhar A, Kumar R, Pandita RK, Bhat KM, Ramos KS, Pandita TK (2022) Role of transposable elements in genome stability: Implications for health and disease. Int J Mol Sci 23: 7802

Black D, Jackson M, Kidwell M, Dover G (1987) KP elements repress P-induced hybrid dysgenesis in Drosophila melanogaster. EMBO J. 6: 4125-4135

Bolger AM, Lohse M, Usadel B (2014) Trimmomatic: A flexible trimmer for Illumina sequence data. Bioinformatics btu170

Brennecke J, Malone C, Aravin A, Sachidanandam R, Stark A, Hannon G (2008) An epigenetic role for maternally inherited piRNAs in transposon silencing. Science 322: 1387-1392

Carpenter R, Martin C, Coen ES (1987) Comparison of genetic behaviour of the transposable element Tam3 at two unlinked pigment loci in Antirrhinum majus. Mol. Gen. Genet. 207: 82-89

Castel S, Martienssen R (2013) RNA interference in the nucleus: roles for small RNAs in transcription, epigenetics and beyond. Nat. Rev. Genet. 14: 100-112

806 Chatterjee M, Martin C (1997) Tam3 produces a suppressible allele of the DAG locus
807 of Antirrhinum majus similar to Mu-suppressible alleles of maize. Plant J 11:
808 759-771
809 Ciechanowska K, Pokornowska M, Kurzyńska-Kokorniak A (2021) Genetic insight
810 into the domain structure and functions of dicer-type ribonucleases. Int J Mol
811 Sci 22: 616
812 Coen ES, Robbins TP, Almeida J, Hudson A, Carpenter R (1989) Consequences and
813 mechanisms of transposition in Antirrhinum majus *In* DE Berg, MM Howe,
814 eds, Mobile DNA. Washington, DC, American Society for Microbiology, pp
815 413-436
816 Cuypers H, Dash S, Peterson P, Saedler H, Gierl A (1988) The defective En-I102
817 element encodes a product reducing the mutability of the En/Spm transposable
818 element system of Zea mays. The EMBO Journal: 2953-2960
819 Erdmann R, Picard CL (2020) RNA-directed DNA methylation. PLOS Genetics 16:
820 e1009034
821 Fedoroff N, Masson P, Banks JA (1989) Mutations, epimutations, and the
822 developmental programming of the maize Suppressor-mutator transposable
823 element. Bioessays 10: 139-144
824 Fincham J, Harrison B (1967) Instability at the pal locus in Antirrhinum majus II.
825 Multiple alleles produced by mutation of one original unstable allele. Heredity
826 22: 211-224
827 Fujino K, Hashida SN, Ogawa T, Natsume T, Uchiyama T, Mikami T, Kishima Y
828 (2011) Temperature controls nuclear import of Tam3 transposase in
829 Antirrhinum. Plant J 65: 146-155
830 Fujino K, Sekiguchi H, Kiguchi T (2005) Identification of an active transposon in
831 intact rice plants. Mol Genet Genomics 273
832 Gierl A (1996) The En/Spm Transposable Element of Maize. *In* H Saedler, A Gierl,
833 eds, Transposable Elements, Vol 204. Springer, Berlin, Heidelberg, Current
834 Topics in Microbiology and Immunology, pp 145-159
835 Harrison B, Carpenter R (1973) A comparison of the instabilities at the nivea and

836 pallida loci in Antirrhinum majus. Heredity 31: 309-323
837 Harrison BJ, Fincham JRS (1964) Instability at the Pal locus in Antirrhinum majus I.
838 Effects of environment on frequencies of somatic and germinal mutation.
839 Heredity 19: 237-258
840 Harrison BJ, Fincham JRS (1968) Instability at the Pal locus in Antirrhinum majus 3.
841 A gene controlling mutation frequency. Heredity 23: 67-72
842 Hashida SN, Uchiyama T, Martin C, Kishima Y, Sano Y, Mikami T (2006) The
843 temperature-dependent change in methylation of the Antirrhinum transposon
844 Tam3 is controlled by the activity of its transposase. Plant Cell 18: 104-118
845 Hehl R, Nacken WK, Krause A, Saedler H, Sommer H (1991) Structural analysis of
846 Tam3, a transposable element from *Antirrhinum majus*, reveals homologies to
847 the Ac element in maize. Plant Mol. Biol. 16: 369-371
848 Inagaki Y, Hisatomi Y, Suzuki T, Kasahara K, lida S (1994) Isolation of a Suppressor-
849 mutator/Enhancer-like transposable element, Tpn1, from Japanese morning
850 glory bearing variegated flowers. The Plant Cell 6: 375-383
851 Ito H (2013) Small RNAs and regulation of transposons in plants. Genes Genet. Syst.
852 88: 3-7
853 Kishima Y, Yamashita S, Martin C, Mikami T (1999) Structural conservation of the
854 transposon Tam3 family in Antirrhinum majus and estimation of the number of
855 copies able to transpose. Plant Mol Biol 39: 299-308
856 Kitamura K, Hashida SN, Mikami T, Kishima Y (2001) Position effect of the excision
857 frequency of the Antirrhinum transposon Tam3: implications for the degree of
858 position-dependent methylation in the ends of the element. Plant Mol Biol 47:
859 475-490
860 Kryovrysanaki N, James A, Tselika M, Bardani E, Kalantidis K (2022) RNA silencing
861 pathways in plant development and defense. Int. J. Dev. Biol. 66: 163-175
862 Lazarow K, Doll ML, Kunze R (2013) Molecular biology of maize Ac/Ds elements:
863 an overview. Methods Mol Biol 1057: 59-82
864 Lee CC, Beall EL, Rio DC (1998) DNA binding by the KP repressor protein inhibits
865 P-element transposase activity in vitro. The EMBO Journal 17: 4166-4174

Levin H, Moran J (2011) Dynamic interactions between transposable elements and their hosts. Nat. Rev. Genet. 12: 615-627

Lisch D (2002) Mutator transposons. Trends Plant Sci. 7: 498-504

Liu P, Cuerda-Gil D, Shahid S, Slotkin RK (2022) The epigenetic control of the transposable element life cycle in plant genomes and beyond. Annu Rev Genet 56: 63-87

Liu YX, Wang M, Wang XJ (2014) Endogenous small RNA clusters in plants. Genomics Proteomics Bioinformatics 12: 64-71

Liyanage VRB, Jarmase JS, Murugeshan N, Bigio MRD, Mojgan R, Davie JR (2014) DNA Modifications: Function and applications in normal and disease states. Biology 3: 670-723

Majumdar S, Rio DC (2015) P transposable elements in Drosophila and other eukaryotic organisms. Microbiol. Spectr. 3: MDNA3-0004

Martin C, Carpenter R, Sommer H, Saedler H, Coen ES (1985) Molecular analysis of instability in flower pigmentation of Antirrhinum majus, following isolation of the pallida locus by transposon tagging. EMBO J. 4: 1625-1630

Mathieu O, Bender J (2004) RNA-directed DNA methylation. J. Cell Sci. 117: 4881-4888

Miller JL, Grant PA (2013) The role of DNA methylation and histone modifications in transcriptional regulation in humans. Subcell Biochem. 61: 289-317

Okamoto H, Hirochika H (2001) Silencing of transposable elements in plants. Trends Plant Sci. 6

Roche S, Rio D (1998) Trans-silencing by P elements inserted in subtelomeric heterochromatin involves the Drosophila Polycomb group gene, Enhancer of zeste. Genetics 149: 1839-1855

Ronsseray S, Lehmann M, Anxolabehere D (1991) The maternally inherited regulation of P elements in Drosophila melanogaster can be elicited by two P copies at cytological site 1A on the X chromosome. Genetics: 501-512

Ronsseray S, Lehmann M, Nouaud D, Anxolabehere D (1996) The regulatory properties of autonomous subtelomeric P elements are sensitive to a

Suppressor of variegation in Drosophila melanogaster. Genetics 143: 1663-1674

Slotkin R, Martienssen R (2007) Transposable elements and the epigenetic regulation of the genome. Nat. Rev. Genet. 8: 272-285

Slotkin RK, Freeling M, Lisch D (2003) Mu killer causes the heritable Inactivation of the Mutator family of transposable elements in Zea mays. Genetics 165: 781-797

Slotkin RK, Freeling M, Lisch D (2005) Heritable transposon silencing initiated by a naturally occurring transposon inverted duplication. Nat Genet 37: 641-644

Statello L, Guo C, Chen L, Huarte M (2021) Gene regulation by long non-coding RNAs and its biological functions. *Nat. Rev. Mol. Biol.* 22: 96-118

Tan Y, Bukys A, Molnár A, Hudson A (2020) Rapid, high efficiency virus-mediated mutant complementation and gene silencing in *Antirrhinum* Plant Methods 16

Uchiyama T, Hiura S, Ebinuma I, Senda M, Mikami T, Martin C, Kishima Y (2013) A pair of transposons coordinately suppresses gene expression, independent of pathways mediated by siRNA in Antirrhinum. New Phytol. 197: 431-440

Uchiyama T, Saito Y, Kuwabara H, Fujino K, Kishima Y, Martin C, Sano Y (2008) Multiple regulatory mechanisms influence the activity of the transposon, Tam3, of Antirrhinum. New Phytol 179: 343-355

Viviani A, Ventimiglia M, Fambrini M, Vangelisti A, Mascagni F, Pugliesi C, Usai G (2021) Impact of transposable elements on the evolution of complex living systems and their epigenetic control. Biosystems 210: 104566

Walbot V, Rudenko GN (2007) MuDR/Mu Transposable Elements of Maize. *In* NL Carig, R Craigie, M Gellert, eds, Monile DNA II. Washington DC, AMS Press, pp 533-564

Wang S, Koide Y, Kishima Y (2022) How to establish a mutually beneficial relationship between a transposon and its host: lessons from Tam3 in Antirrhinum Genes Genet. Syst. 97: 177-184

Yoo S-D, Cho Y-H, Sheen J (2007) Arabidopsis mesophyll protoplasts: A versatile cell system for transient gene expression analysis. Nat Protoc 2: 1565-1572

Zhong C, Smith NA, Zhang D, Goodfellow S, Zhang R, Shan W, Wang MB (2019) Full-Length hairpin RNA accumulates at high levels in yeast but not in bacteria and plants. Genes (Basel) 10: 458

Zhou H, Hirata M, Osawa R, Fujino K, Kishima Y (2017) Detainment of Tam3 transposase at plasma membrane by its BED-Zinc finger domain. Plant Physiol 173: 1492-1501

Figure legends

Fig. 1

OSt suppresses Tam3 transposition.

A. Profiles of *ost*/*niv*^{rec} (HAM2) and *OSt*/*niv*^{rec} (HAM21) *A. majus* lines. The two lines share the *niv*^{rec} allele at *Niv* locus encoding chalcone synthase (CHS), where a Tam3 element is inserted in the promoter of *CHS* gene. Tam3 insertion can restrict the expression of *CHS* gene in *niv*^{rec}, which thus gives rise to the flower petals with pale red background at 25℃. *ost*/*niv*^{rec} (HAM2) does not contain suppressors for Tam3 transposition and thus exhibits red sites and sectors on flower petals at 15℃ due to Tam3 transposition. *OSt* suppressor is carried in the *OSt*/*niv*^{rec} (HAM21) genome and strongly suppresses Tam3 transposition, which eventually causes a few red sectors on flower petals at 15℃. Additionally, PCR analysis using F and R primers to examine Tam3 transposition showed that Tam3 is inactive at 25℃, and 2.0 kb Tam3-excision bands were missing in *ost*/*niv*^{rec} (HAM2) and *OSt*/*niv*^{rec} (HAM21). At 15℃, Tam3 is active in *ost*/*niv*^{rec} (HAM2), and the excision bands can be observed, but not in *OSt*/*niv*^{rec} (HAM21). B. The chromosomal position of *OSt*. C. Structural comparison between Tam3 on *niv*^{rec} and *OSt*-Tam3.

Fig. 2

NSt suppresses Tam3 transposition.

A. Profiles of *nst*/*niv*$^{rec:\ beni}$ (HAM5) and *NSt*/*niv*$^{rec:\ beni}$ (HAM3) *A. majus* lines. The two lines share the *niv*$^{rec:\ beni}$ allele at *Niv* locus, where two Tam3 elements are inserted

into the promoter and downstream of *CHS* gene, respectively. Tam3 strongly restricts the expression of *CHS* gene at *niv*$^{rec:\ beni}$ allele, which causes light-colored flower petals at 25℃. *nst*/*niv*$^{rec:\ beni}$ (HAM5) does not contain suppressors for Tam3 transposition and thus exhibits red sites and sectors on flower petals at 15℃ due to Tam3 transposition. *NSt* suppressor resides in *NSt*/*niv*$^{rec:\ beni}$ (HAM3) genome and strongly suppress Tam3 transposition, which results in no variegations on flower petals at 15℃. The 2.0 kb Tam3-excision band was not observed in the two lines at 25℃ and *NSt*/*niv*$^{rec:\ beni}$ (HAM3) at 15℃, but was observed in *nst*/*niv*$^{rec:\ beni}$ (HAM5) at 15℃. B. The chromosomal position and structure of *NSt*.

Fig. 3

Nuclear import and Tam3 DNA binding of Tam3 TPase.

A. Plasma membrane and nuclear localization of Tam3 TPase in *Antirrhinum* protoplasts. B. The proportions of cells with Tam3 TPase-GFP signals in nuclei out of total number of cells with fluorescence (Supplementary Table 2). Data represent means ± SD. Significant differences were determined by Student's t-test. C. Immunoblot analysis of total, cytoplastic and nuclear protein. The fragments indicated by upper and lower arrows correspond to 100 kDa of Tam3 TPase and 17 kDa of H3 Histone, respectively. The plus (+) and minus (-) marks represent the presence and absence of each protein in each lane, respectively. D. EMSA analysis of DNA binding ability of nuclear Tam3 TPase. Nucleotide sequence of Tam3: 79-104 in Tam3 containing three GCHCG motifs, was used as a probe. The probe and nuclear protein are mixed with 50 fM and 2 ug, respectively. Shifted bands from free probes (bottom two bands) were detected in *OSt*, *NSt* and *ost*/*nst* plants grown at 15℃ when nuclear protein was added (+). While absence of nuclear protein (−), no shifted bands appeared.

Fig. 4

Distributions and amounts of total small RNAs in 5' region of intact Tam3.

To employ the same mapping approach in the three genotypes because of several

SNPs exist in the 5' rearranged region of *OSt*-Tam3, thus the mapping was carried out as follows: sRNAs firstly were perfectly matched to Tam3 (1-3633 bp), and remained sRNAs were then collected and finally perfectly aligned to *OSt*-Tam3 (1-3919 bp). sRNAs in the first step and sRNAs perfectly aligned to the 5' 1-201 bp region of *OSt*-Tam3 were combined together, and then 21, 22 and 24 nt sRNAs were selected respectively and simply combined together as total sRNAs. The total sRNAs were divided into two strands: the sense and antisense strands of Tam3, and then these sRNAs matched to the 5' 1-201 bp region of Tam3 were analyzed in *OSt*, *NSt* and *ost*/*nst*. Red and blue squares on nucleotide sequences indicate Terminal Inverted Repeat (TIR) and GCHCG motifs, respectively. The lines above the DNA sequence indicate as follows; blue: *OSt* (HAM21), red: *NSt* (HAM3), black: *ost*/*nst* (HAM5). Black and brown lines below the DNA sequence represent "x" and "y" regions of intact Tam3, respectively. RPH, reads per hundred mapped reads.

Fig. 5

Possible double-stranded RNAs derived from *OSt* and *NSt*.

A. Possible double-stranded RNAs derived from *OSt*. The two highest combinations of sense and antisense transcriptional start sites were represented in *OSt* (Supplementary Table 3). The transcription on the sense and antisense strands of *OSt* DNA fragment causes the production of sense and antisense transcripts which are paired to form double-stranded RNA. B. Possible double-stranded RNAs derived from *NSt*. One sense transcriptional start site was represented in *NSt*. The transcription starts from the 5' end of Tam3-L and goes through to the 5' end of Tam3-R. The transcript contains two paired parts at the two ends and thus can be folded into stem-loop structure where dsRNA exists in stem part. Red and blue vertical fold arrows represent predicted transcriptional start sites on sense and antisense strands of *OSt* and *NSt*, respectively. The number in parenthesis represents the nucleotide position of TSS from the left side of *OSt* or *NSt*. TSS, transcriptional start site.

Fig. 6

Tam3 sRNA induction in *nst*/*ost* plants by VIGS.

A. Leaf variegation phenotype in *ost*/*nst Antirrhinum* plants inoculated with TRV carrying 242 bp of 5' terminal Tam3 fragment in sense orientation (TRV-Tam3) and TRV (mock), and without TRV, respectively. 21 days-old *ost*/*nst* plants inoculated with TRV-Tam3, TRV and without TRV were grown at 15℃ for at least two weeks. These plants exhibited different variegation phenotypes on the leaves. B. Detection of transcripts from *CP* gene to the Tam3 fragment in TRV-Tam3-inoculated plants. Tam3 sRNAs production requires the transcription of precusor RNA which is from *CP* gene to inserted 1-242 bp Tam3 5' fragment (Supplementary Fig. 22B). Amplification of *UBIQ* gene was used as a control for cDNA. And amplification of *CP* gene in mock-inoculated plant was used as negative control. Above structure diagram represents the functional section responsible for sRNA induction in TRV2 RNA plasmid. Small arrows indicate the positions of primers using for *CP*-Tam3 transcripts. Primer sequences were present in Supplementary Table 4. C. Distributions and amounts of total sRNAs in 5' terminal region of Tam3 sequence in TRV-Tam3-inoculated plants. Aligned sRNAs reads filtered with zero or one mismatch were analyzed. 21, 22, 23 and 24 nt sRNAs were selected respectively and simply combined as total sRNAs. In the structure diagram of 5' terminal region of Tam3 sequence, red and blue squares represent the Terminal Inverted Repeat (TIR) and GCHCG motifs, respectively. RPM: reads per million sequenced reads. D. Relative excision rates of Tam3 copy at niv^{rec} and *S78* loci in TRV-Tam3- and mock-inoculated plants and plants without TRV inoculation. Data represents means ± SD. Band intensity was measured by ImageJ. Significant differences were determined by Dunnett's test. Single and double asterisks represent the significant and extremely significant differences, respectively.

Fig. 7

OSt and *NSt* suppress Tam3 transposition by two possible mechanisms.

Transcription of *OSt* and *NSt* DNA fragments can result in the production of double-stranded RNAs which can be processed into sRNAs. Certain proteins carry these sRNAs and transport them into nucleus. In the nucleus, the sRNAs may bind to the

antisense strand of 5' end of Tam3 DNA (A) or interact with Tam3 TPase itself (B) to inhibit the binding between Tam3 TPase and Tam3 DNA, which results in the suppression of Tam3 transposition.

Supplementary Figure legends

Supplementary Fig. 1

Profile of wild type (WT) *A. majus* line.

WT contains the *Niv* allele at *Niv* locus, where no Tam3 is inserted, and thus the flower petals exhibit red color at 25℃ and 15℃. Additionally, the observation of 2.0 kb bands at 25℃ and 15℃ indicates no Tam3 insertion in the *Niv* allele.

Supplementary Fig. 2

F2 segregation profiles in the *OSt*/*niv*^{rec} × *ost*/*niv*^{rec} (HAM21×HAM2) and *NSt*/*niv*$^{rec:\ beni}$ × *nst*/*niv*$^{rec:\ beni}$ (HAM3×HAM5) *Antirrhinum* crosses.

A. F2 segregation in the *OSt*/*niv*^{rec} × *ost*/*niv*^{rec} (HAM21×HAM2) cross. B. F2 segregation in the *NSt*/*niv*$^{rec:\ beni}$ × *nst*/*niv*$^{rec:\ beni}$ (HAM3×HAM5) cross. The number of plants showing different spotted phenotypes in F2 is shown in Supplementary Table 1.

Supplementary Fig. 3

Chromosomal positions of *OSt*, *NSt*, *Niv* and *Pal* within the *Antirrhinum majus* genome.

Supplementary Fig. 4

Identification of *OSt*.

A. Transposon tagging analysis in *ost*/*niv*^{rec} (HAM2), *OSt*/*niv*^{rec} (HAM21) and their progeny plants. Each DNA was extracted and digested with *Eco*RI. The ORF region of Tam3 was used as a probe, and black arrow indicates the 6.6 kb "tag" bands in *OSt*/*niv*^{rec} (HAM21), F1 and middle-spotted F2 plants. B. Different flower variegation phenotypes of plants used for the identification of *OSt*. C. Structures of *OSt* and *ost*

alleles. The two thin vertical bars in *OSt* represent *Eco*RI sites. Arrows represent the positions of primers present in *OSt* and *ost* alleles. D. PCR analysis of the allelic constitution at *OSt* locus in plants with different flower petal variegation phenotypes. The A (1.5 kb) fragment amplified using the F2 and R primers indicates the *OSt* allele, while the B (3.0 kb) fragment amplified using the F1 and R primers indicates the *ost* allele.

Supplementary Fig. 5

Dot plot analysis and sequence alignment of the *OSt* sequence.

A. *OSt* sequence was aligned to the intact Tam3 sequence from *niv*^{rec}. In the dot plot, the upper horizontal axis represents *OSt* sequence, and left vertical axis represents the Tam3 sequence. Red and green dots represent the alignment of the sequence of positive and negative strands of *OSt* to the sequence of the positive strand of Tam3, respectively. The window size and mismatch limit settings in dot plot analysis are 10 and 0, respectively. B. Sequence alignment between x-y-z region of intact Tam3 and x'-y'-z'-x''-z'' region of *OSt*-Tam3. Black and blue squares indicate SNP and deletion positions, respectively. Red and black underlines indicate Terminal Inverted Repeat (TIR) and GCHCG motifs, respectively.

Supplementary Fig. 6

Identification of *NSt*.

A. Transposon tagging analysis in low- and high-spotted plants. Each DNA was extracted and digested with *Eco*RV. Full-length Tam3 sequence was used as a probe, and black arrow indicated 3.5 kb tagging bands in low-spotted plants. B. Different flower variegation phenotypes of plants used for the identification of *NSt*. C. Structures of *NSt* and *nst* alleles. Vertical bars indicate the nucleotide positions of restriction enzymes including *Eco*RV, *Bgl*I and *Xba*I in *NSt* and *nst* alleles. The bold black line below *nst* in the diagram represents the probe used for Southern blotting analysis. D. Southern blotting analysis of allelic constitution at *NSt* locus in plants with different flower petal variegation phenotypes. Each DNA was extracted and

digested with *Eco*RV. The probe used is shown in the C diagram. The 3.5 kb fragment was detected in low-spotted plants and indicates the *NSt* allele, while the 2.7 kb fragment was detected in high-spotted plants and indicates the *nst* allele.

Supplementary Fig. 7

Dot plot analysis of the *NSt* sequence and the process of *NSt* formation.

A. *NSt* sequence was aligned to the intact Tam3 sequence from *niv*^{rec}. In the dot plot, the upper horizontal axis represents *NSt* sequence, and the left vertical axis represents the Tam3 sequence. Red and green dots represent the alignment of the sequence of positive and negative strands of *OSt* to the sequence of positive strand of Tam3, respectively. The window size and mismatch limit settings for the dot plot analysis were 10 and 0, respectively. B. Proposed process of *NSt* formation. One Tam3 element was inserted into the third intron of *Am02g32060* gene, which results in *nst* formation. *NSt* formation was due to the insertion of second Tam3 element on the right side of first Tam3 element in the same intron.

Supplementary Fig. 8

The transcription and translation of *Tam3 TPase*.

A. qRT-PCR analysis of *Tam3 TPase* expression. Expression levels were normalized to that of *UBIQ* (X67957). Data represent the means ± SD (n = 3). Significant differences were determined by Dunnett's test. The experiments were performed three times. B. Immunoblot analysis of Tam3 TPase in the same plants employed with the qRT-PCR analysis. Total protein was extracted from young leaves of *Antirrhinum* plants. The fragments indicated by arrows correspond to 100 kDa of Tam3 TPase. C. CBB staining of SDS-gel for total protein in the immunoblot analysis. Black dot squares mark the range of the B immunoblot membrane figures in the SDS-gel.

Supplementary Fig. 9

Distributions and amounts of mRNAs in Tam3 region.

The mRNAs that were perfectly matched to the Tam3 region (1-3633 bp) were

analyzed. Red and blue colors were used to distinguish sense and antisense mRNAs, respectively. The vertical fold arrow in the Tam3 structure diagram represents the transcriptional start site of *Tam3 TPase* gene. ATG and TAA are start and stop codons of Tam3 TPase, respectively. FPH, fragments per hundred mapped fragments.

Supplementary Fig. 10

Distributions and amounts of mRNAs in Tam3 and *OSt*-Tam3 regions in *OSt*/*niv*^{rec} (HAM21).

The mRNAs that perfectly matched were aligned to the Tam3 region (1-3633 bp) and the *OSt*-Tam3 region (1-3919 bp) in *OSt*/*niv*^{rec} (HAM21). Red and blue colors were used to distinguish sense and antisense mRNAs, respectively. The vertical fold arrow in the Tam3 structure diagram represents the transcriptional start site of the *Tam3 TPase* gene. ATG and TAA are start and stop codons of Tam3 TPase, respectively. FPH, fragments per hundred mapped fragments.

Supplementary Fig. 11

Distributions and amounts of mRNAs in *NSt* and *nst* alleles.

The mRNAs that perfectly matched were aligned to the 5' region of Tam3-L of *nst* (1-689 bp) and the flanking region of Tam3-L of *nst* (1867 bp) in *nst*/*niv*$^{rec:\ beni}$ (HAM5), and aligned to 5' regions of Tam3-L (1-689 bp) and Tam3-R (1-689 bp) of *NSt* and internal region (1867 bp) between Tam3-L and Tam3-R of *NSt* in *NSt*/*niv*$^{rec:\ beni}$ (HAM3). Red and blue colors were used to distinguish sense and antisense mRNAs, respectively. FPH, fragments per hundred mapped fragments.

Supplementary Fig. 12

Distributions and amounts of RNAs (lncRNAs + mRNAs) in the Tam3 region.

The RNAs including lncRNAs and mRNAs that were perfectly matched to the Tam3 region (1-3633 bp) were analyzed. Red and blue colors were used to distinguish sense and antisense RNAs, respectively. The vertical fold arrow in the Tam3 structure diagram represents the transcriptional start site of the *Tam3 TPase* gene. ATG and

TAA are start and stop codons of the Tam3 TPase, respectively. FPH, fragments per hundred mapped fragments.

Supplementary Fig. 13

Distributions and amounts of RNAs (lncRNAs + mRNAs) in Tam3 and *OSt*-Tam3 regions in *OSt*/*niv*^{rec} (HAM21).

The RNAs including lncRNAs and mRNAs that perfectly matched were aligned to the Tam3 region (1-3633 bp) and the *OSt*-Tam3 region (1-3919 bp) in *OSt*/*niv*^{rec} (HAM21). Red and blue colors were used to distinguish sense and antisense RNAs, respectively. The vertical fold arrow in the Tam3 structure diagram represents the transcriptional start site of the *Tam3 TPase* gene. ATG and TAA are start and stop codons of the Tam3 TPase, respectively. FPH, fragments per hundred mapped fragments.

Supplementary Fig. 14

Distributions and amounts of RNAs (lncRNAs + mRNAs) in *NSt* and *nst* alleles.

The RNAs including lncRNAs and mRNAs that perfectly matched were aligned to the 5' region of Tam3-L of *nst* (1-689 bp) and the flanking region of Tam3-L of *nst* (1867 bp) in *nst*/*niv*$^{rec:\ beni}$ (HAM5), and aligned to the 5' regions of Tam3-L (1-689 bp) and Tam3-R (1-689 bp) of *NSt* and the internal region (1867 bp) between Tam3-L and Tam3-R of *NSt* in *NSt*/*niv*$^{rec:\ beni}$ (HAM3). Red and blue colors were used to distinguish sense and antisense RNAs, respectively. FPH, fragments per hundred mapped fragments.

Supplementary Fig. 15

Distributions and amounts of sense sRNAs in the Tam3 region.

To employ the same mapping approach in the three genotypes because of several SNPs exist in the 5' rearranged region of *OSt*-Tam3, thus the mapping was carried out as follows: sRNAs firstly were perfectly matched to Tam3 (1-3633 bp), and remained sRNAs were then collected and finally perfectly aligned to *OSt*-Tam3 (1-3919 bp).

sRNAs in the first step and sRNAs perfectly aligned to the 5' 1-201 bp region of *OSt*-Tam3 were combined together, and then 21, 22 and 24 nt sRNAs were selected respectively and simply combined together as total sRNAs. The 21, 22, 24 nt and total sRNAs were divided into two strands: the sense and antisense strands of Tam3, and then 21-22, 24 nt and total sRNAs on the sense strand were analyzed in *OSt*, *NSt* and *ost*/*nst*, respectively. The vertical fold arrow and red vertical line in the Tam3 structure diagram represent the transcriptional start site of the *Tam3 TPase* gene and the position of the GCHCG motif, respectively. ATG and TAA are start and stop codons of the Tam3 TPase, respectively. RPH, reads per hundred mapped reads.

Supplementary Fig. 16

Distributions and amounts of antisense sRNAs in the Tam3 region.

To employ the same mapping approach in the three genotypes because of several SNPs exist in the 5' rearranged region of *OSt*-Tam3, thus the mapping was carried out as follows: sRNAs firstly were perfectly matched to Tam3 (1-3633 bp), and remained sRNAs were then collected and finally perfectly aligned to *OSt*-Tam3 (1-3919 bp). sRNAs in the first step and sRNAs perfectly aligned to the 5' 1-201 bp region of *OSt*-Tam3 were combined together, and then 21, 22 and 24 nt sRNAs were selected respectively and simply combined together as total sRNAs. The 21, 22, 24 nt and total sRNAs were divided into two strands: the sense and antisense strands of Tam3, and then 21-22, 24 nt and total sRNAs on the antisense strand were analyzed in *OSt*, *NSt* and *ost*/*nst*, respectively. The vertical fold arrow and red vertical line in the Tam3 structure diagram represent the transcriptional start site of the *Tam3 TPase* gene and the position of GCHCG motif, respectively. ATG and TAA are start and stop codons of the Tam3 TPase, respectively. RPH, reads per hundred mapped reads.

Supplementary Fig. 17

Distributions and amounts of total sRNAs in 3' region of intact Tam3.

To employ the same mapping approach in the three genotypes because of several SNPs exist in the 5' rearranged region of *OSt*-Tam3, thus the mapping was carried out

as follows: sRNAs firstly were perfectly matched to Tam3 (1-3633 bp), and remained sRNAs were then collected and finally perfectly aligned to *OSt*-Tam3 (1-3919 bp). sRNAs in the first step and sRNAs perfectly aligned to the 5' 1-201 bp region of *OSt*-Tam3 were combined together, and then 21, 22 and 24 nt sRNAs were selected respectively and simply combined together as total sRNAs. The total sRNAs were divided into two strands: the sense and antisense strands of Tam3, and then these sRNAs perfectly matched to 3' region of Tam3 (3433-3633 bp) were analyzed in *OSt*, *NSt* and *ost*/*nst*. Red and blue squares on nucleotide sequences indicate Terminal Inverted Repeat (TIR) and GCHCG motifs, respectively. Lines indicate as follows; blue: *OSt* (HAM21), red: *NSt* (HAM3), black: *ost*/*nst* (HAM5). RPH, reads per hundred mapped reads.

Supplementary Fig. 18

Distributions and amounts of sRNAs in *OSt*-Tam3 region.

sRNAs that were perfectly matched to the *OSt*-Tam3 region (1-3919 bp) were analyzed. Red and blue colors were used to distinguish sense and antisense sRNAs, respectively. RPH, reads per hundred mapped reads.

Supplementary Fig. 19

Distributions and amounts of sRNAs in 5' regions of Tam3, *OS*t-Tam3 and Tam3 of *nst* and *NSt*.

A. Distributions and amounts of sRNAs in 5' x-y-z region of Tam3 in *nst*/*niv*$^{\text{rec: beni}}$ (HAM5). B. Distributions and amounts of sRNAs in 5' x'-y'-z'-x''-z'' region of *OSt*-Tam3 in *OSt*/*niv*$^{\text{rec}}$ (HAM21). C. Distributions and amounts of sRNAs in the 5' region of Tam3-L of *nst* (540-689 bp) and flanking region of Tam3-L of *nst* (690-740 bp) in *nst*/*niv*$^{\text{rec: beni}}$ (HAM5). D. Distributions and amounts of sRNAs in the 5' regions of Tam3-L (540-689 bp) and Tam3-R (2557-2705 bp) of *NSt* and flanking regions of Tam3-L (690-740 bp) and Tam3-R (2505-2556 bp) in *NSt*/*niv*$^{\text{rec: beni}}$ (HAM3). sRNAs that perfectly matched were aligned to the regions. Gray, red and blue squares on nucleotide sequences indicate Target Site Duplication (TSD), Terminal Inverted

Repeat (TIR) and GCHCG motifs, respectively. Lines indicate as follows; blue: total sRNAs, green: 24nt sRNAs, black: 22nt sRNAs and red: 21nt sRNAs. RPH, reads per hundred mapped reads.

Supplementary Fig. 20

Detection of a possible hairpin transcript in the *NSt* and *nst* alleles.

In panel A, the F1 and R1 primers amplified a 0.8 kb PCR fragment in the DNA and cDNA samples with the *NSt* allele and DNA sample with *nst* allele, but not in the RNA direct sample with the *NSt* allele and RNA samples with the *nst* allele. Panel B shows a 1.5 kb PCR fragment amplified with the DNA and cDNA of *NSt* and *nst* alleles using F2 and R2 primers. F1 and R1 are located at the 5' end of both Tam3-L and Tam3-R. F2 and R2 primers are presented in the internal region between two Tam3 elements of *NSt* (1-1867 bp). Supplementary Table 4 shows the primer sequences. M indicates the lane of size marker for PCR and RT-PCR products in panel A and B.

Supplementary Fig. 21

Detection of Tam3 excision events at *niv*^{rec} and *S78* loci in TRV-Tam3- and Mock-inoculated plants and plants without TRV inoculation.

The amplification of *DFR* gene at *Pallida* locus was used as a control for Tam3 excision events because of no Tam3 insertion at *Pallida* locus. The vertical fold arrows in *Pal* and *niv*^{rec} structures represent the transcriptional start sites of *DFR* and *CHS* gene, respectively. The red boxes in *Pal* and *niv*^{rec} structures represent the exons of *DFR* and *CHS* gene, respectively. Small arrows indicate the positions of primer using for Tam3 excision detection in the loci. And big arrows above the triangle in *niv*^{rec} and *S78* structures show the direction of inserted Tam3 element. Supplementary Table 4 show the primer sequences. M indicates the lane of size marker for PCR products in the left-side gel figures.

Supplementary Fig. 22

Profiles of TRV-mediated VIGS.

A. Construction of TRV RNA2 plasmid carrying Tam3 fragment. The 242 bp of 5' terminal Tam3 fragment (1st nt to 242nd nt) was amplified and cloned into the TRV RNA2 vector between BamHI and KpnI restriction sites. B. Mechanism of TRV-mediated VIGS. The model figure was modified from Shi *et al.* (2021). Virus ssRNA was transcribed from virus ssDNA inserted with desired fragment, and then RdRP protein syntheses the complementary ssRNA using virus ssRNA as a template to produce dsRNA. The dsRNA was cleaved into sRNAs by Dicer protein, and then RISC binds to the sRNAs as a whole to degrade target mRNAs.

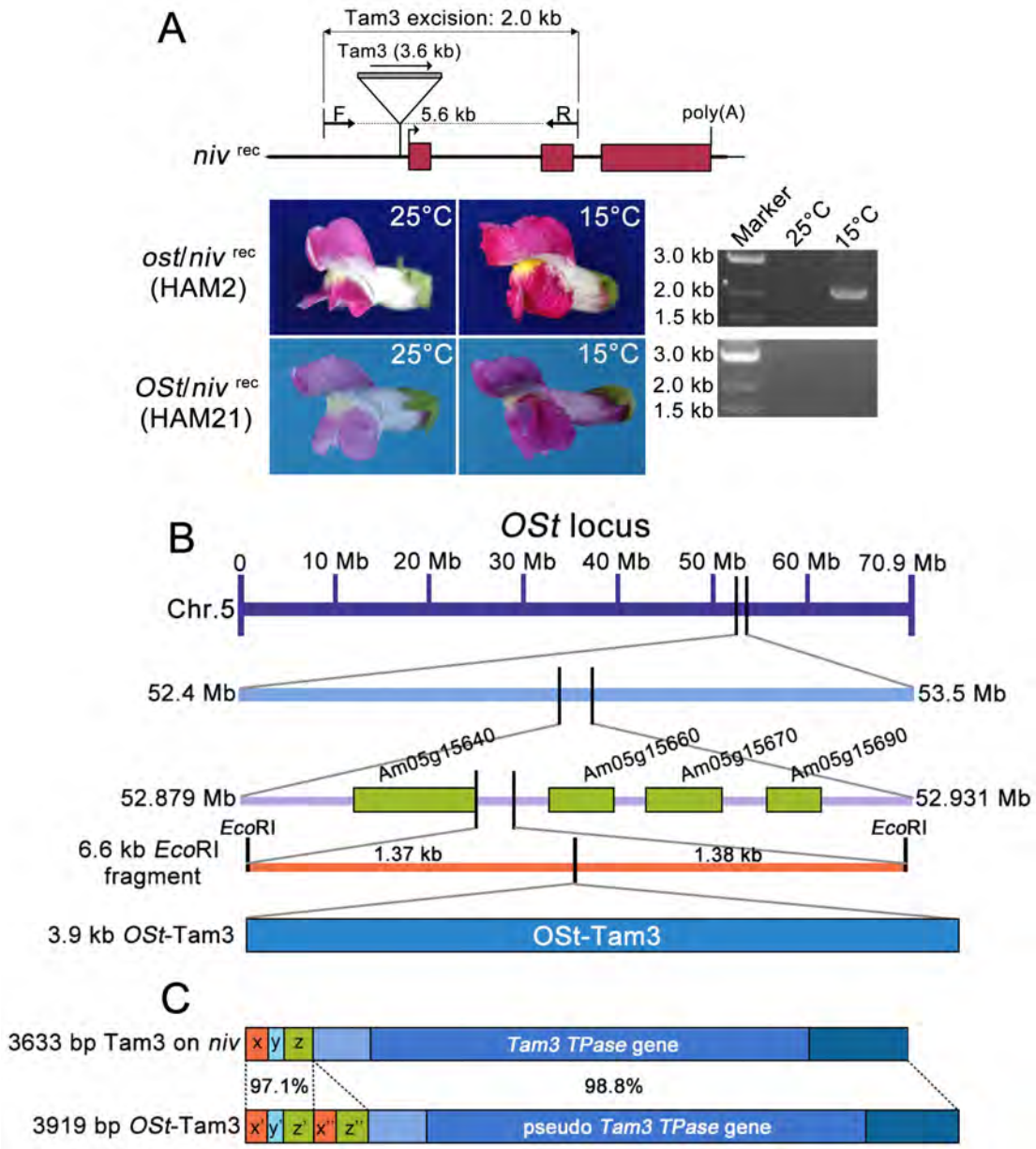


Fig. 1

OSt suppresses Tam3 transposition.

A. Profiles of *ost*/*niv*^{rec} (HAM2) and *OSt*/*niv*^{rec} (HAM21) *A. majus* lines. The two lines share the *niv*^{rec} allele at *Niv* locus encoding chalcone synthase (CHS), where a Tam3 element is inserted in the promoter of *CHS* gene. Tam3 insertion can restrict the expression of *CHS* gene in *niv*^{rec}, which thus gives rise to the flower petals with pale red background at 25°C. *ost*/*niv*^{rec} (HAM2) does not contain suppressors for Tam3 transposition and thus exhibits red sites and sectors on flower petals at 15°C due to Tam3 transposition. *OSt* suppressor is carried in the *OSt*/*niv*^{rec} (HAM21) genome and strongly suppresses Tam3 transposition, which eventually causes a few red sectors on flower petals at 15°C. Additionally, PCR analysis using F and R primers to examine Tam3 transposition showed that Tam3 is inactive at 25°C, and 2.0 kb Tam3-excision bands were missing in *ost*/*niv*^{rec} (HAM2) and *OSt*/*niv*^{rec} (HAM21). At 15°C, Tam3 is active in *ost*/*niv*^{rec} (HAM2), and the excision bands can be observed, but not in *OSt*/*niv*^{rec} (HAM21). B. The chromosomal position of *OSt*. C. Structural comparison between Tam3 on *niv*^{rec} and *OSt*-Tam3.

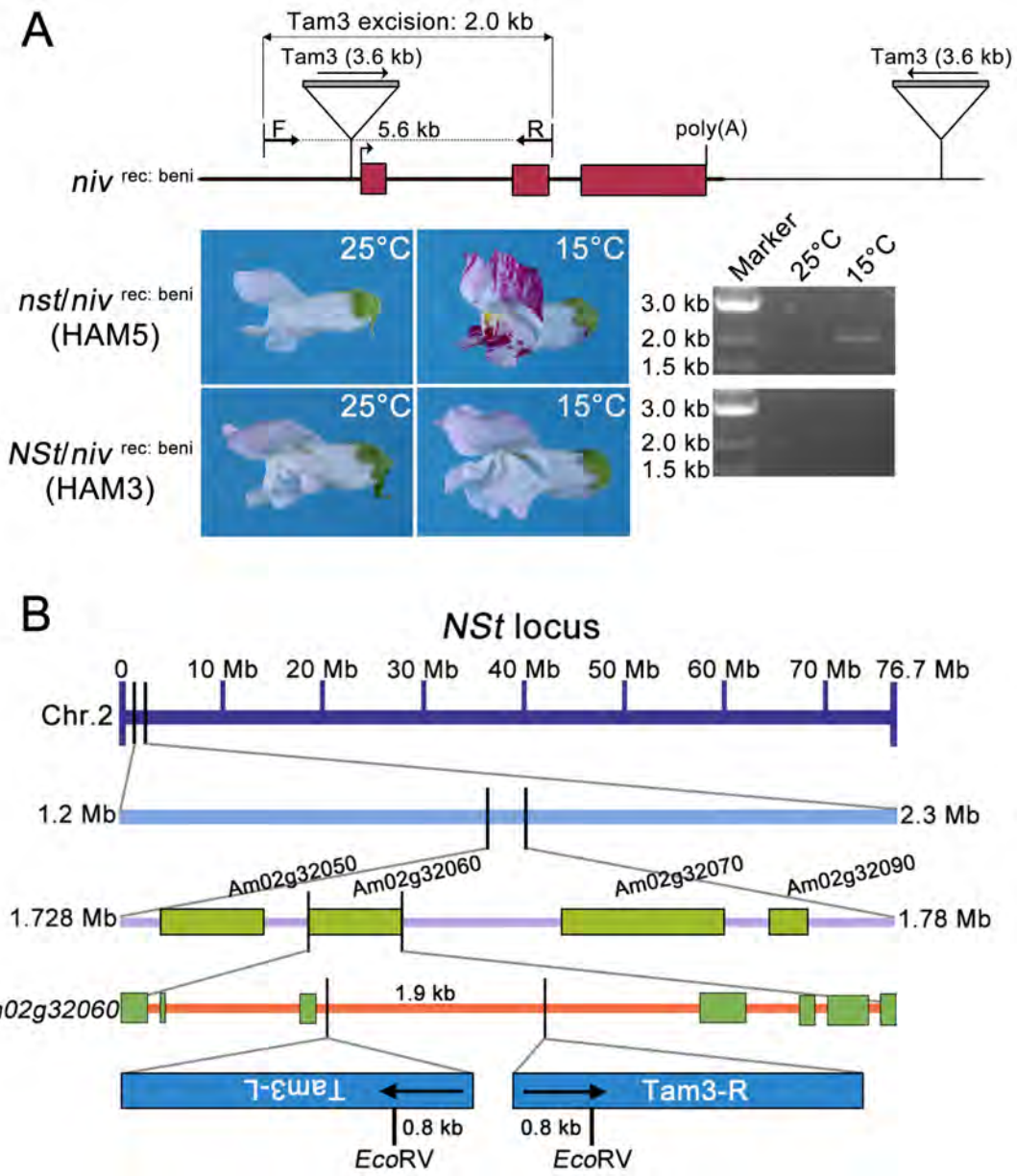


Fig. 2

NSt suppresses Tam3 transposition.

A. Profiles of *nst*/*niv*$^{\text{rec: beni}}$ (HAM5) and *NSt*/*niv*$^{\text{rec: beni}}$ (HAM3) *A. majus* lines. The two lines share the *niv*$^{\text{beni}}$ allele at *Niv* locus, where two Tam3 elements are inserted into the promoter and downstream of *CHS* gene, respectively. Tam3 strongly restricts the expression of *CHS* gene at *niv*$^{\text{rec: beni}}$ allele, which causes light-colored flower petals at 25°C. *nst*/*niv*$^{\text{rec: beni}}$ (HAM5) does not contain suppressors for Tam3 transposition and thus exhibits red sites and sectors on flower petals at 15°C due to Tam3 transposition. *NSt* suppressor resides in *NSt*/*niv*$^{\text{rec: beni}}$ (HAM3) genome and strongly suppress Tam3 transposition, which results in no variegations on flower petals at 15°C. The 2.0 kb Tam3-excision band was not observed in the two lines at 25°C and *NSt*/*niv*$^{\text{rec: beni}}$ (HAM3) at 15°C, but was observed in *nst*/*niv*$^{\text{rec: beni}}$ (HAM5) at 15°C. B. The chromosomal position and structure of *NSt*.

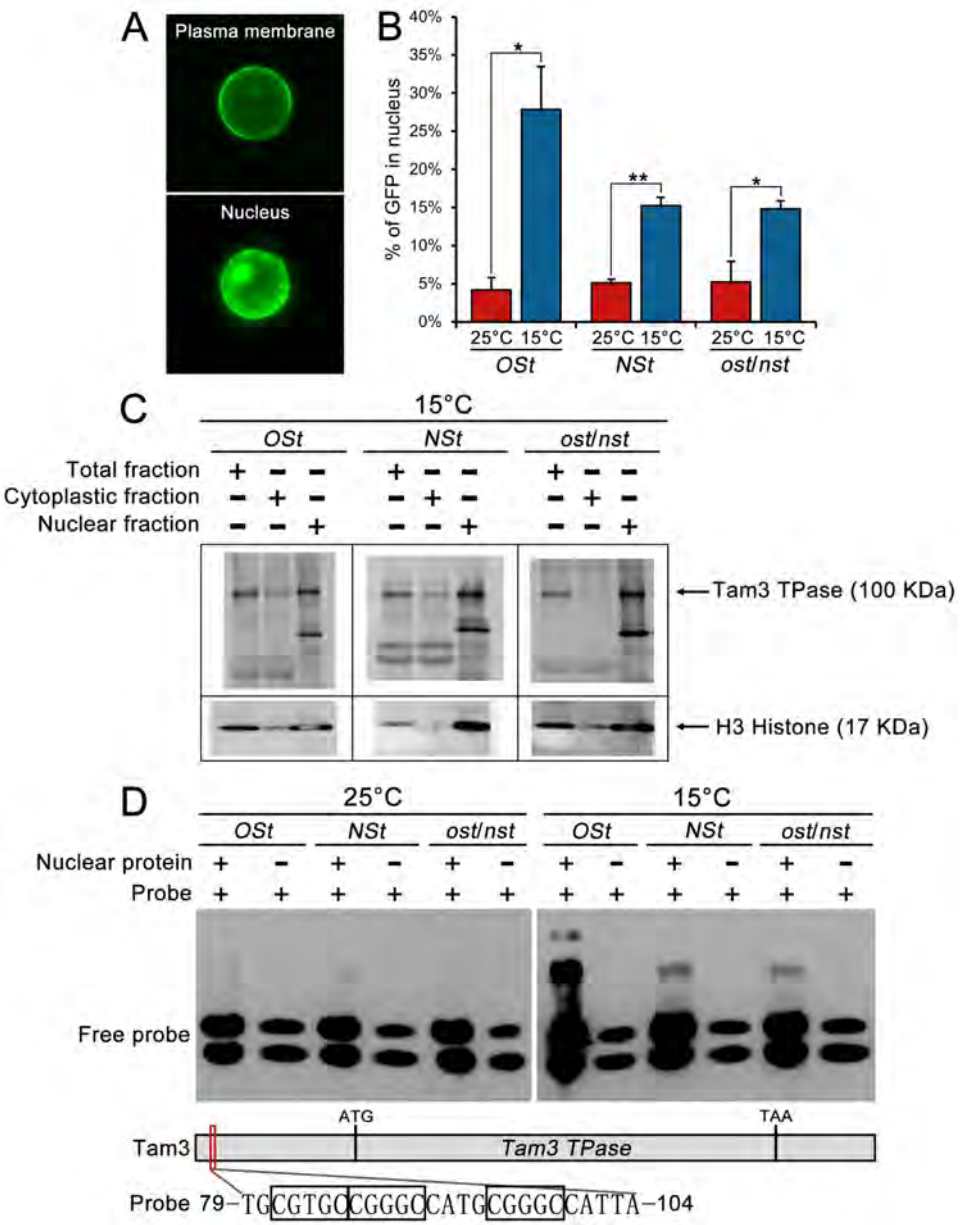


Fig. 3

Nuclear import and Tam3 DNA binding of Tam3 TPase.

A. Plasma membrane and nuclear localization of Tam3 TPase in *Antirrhinum* protoplasts. B. The proportions of cells with Tam3 TPase-GFP signals in nuclei out of total number of cells with fluorescence (Supplementary Table 2). Data represent means ± SD. Significant differences were determined by Student's t-test. C. Immunoblot analysis of total, cytoplastic and nuclear protein. The fragments indicated by upper and lower arrows correspond to 100 kDa of Tam3 TPase and 17 kDa of H3 Histone, respectively. The plus (+) and minus (-) marks represent the presence and absence of each protein in each lane, respectively. D. EMSA analysis of DNA binding ability of nuclear Tam3 TPase. Nucleotide sequence of Tam3: 79-104 in Tam3 containing three GCHCG motifs, was used as a probe. The probe and nuclear protein are mixed with 50 fM and 2 ug, respectively. Shifted bands from free probes (bottom two bands) were detected in *OSt*, *NSt* and *ost*/*nst* plants grown at 15°C when nuclear protein was added (+). While absence of nuclear protein (−), no shifted bands appeared.

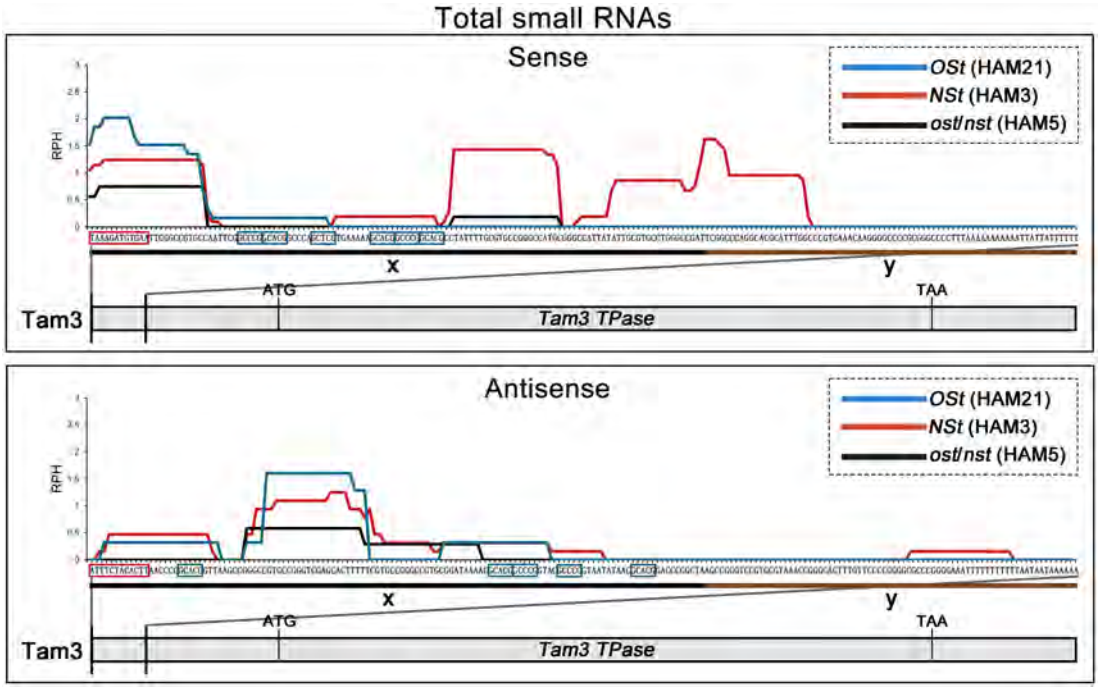


Fig. 4

Distributions and amounts of total small RNAs in 5' region of intact Tam3.

To employ the same mapping approach in the three genotypes because of several SNPs exist in the 5' rearranged region of *OSt*-Tam3, thus the mapping was carried out as follows: sRNAs firstly were perfectly matched to Tam3 (1-3633 bp), and remained sRNAs were then collected and finally perfectly aligned to *OSt*-Tam3 (1-3919 bp). sRNAs in the first step and sRNAs perfectly aligned to the 5' 1-201 bp region of *OSt*-Tam3 were combined together, and then 21, 22 and 24 nt sRNAs were selected respectively and simply combined together as total sRNAs. The total sRNAs were divided into two strands: the sense and antisense strands of Tam3, and then these sRNAs matched to the 5' 1-201 bp region of Tam3 were analyzed in *OSt*, *NSt* and *ost*/*nst*. Red and blue squares on nucleotide sequences indicate Terminal Inverted Repeat (TIR) and GCHCG motifs, respectively. Lines indicate as follows; blue: *OSt* (HAM21), red: *NSt* (HAM3), black: *ost*/*nst* (HAM5). Black and brown lines below the DNA sequence represent "x" and "y" regions of intact Tam3, respectively. RPH, reads per hundred mapped reads.

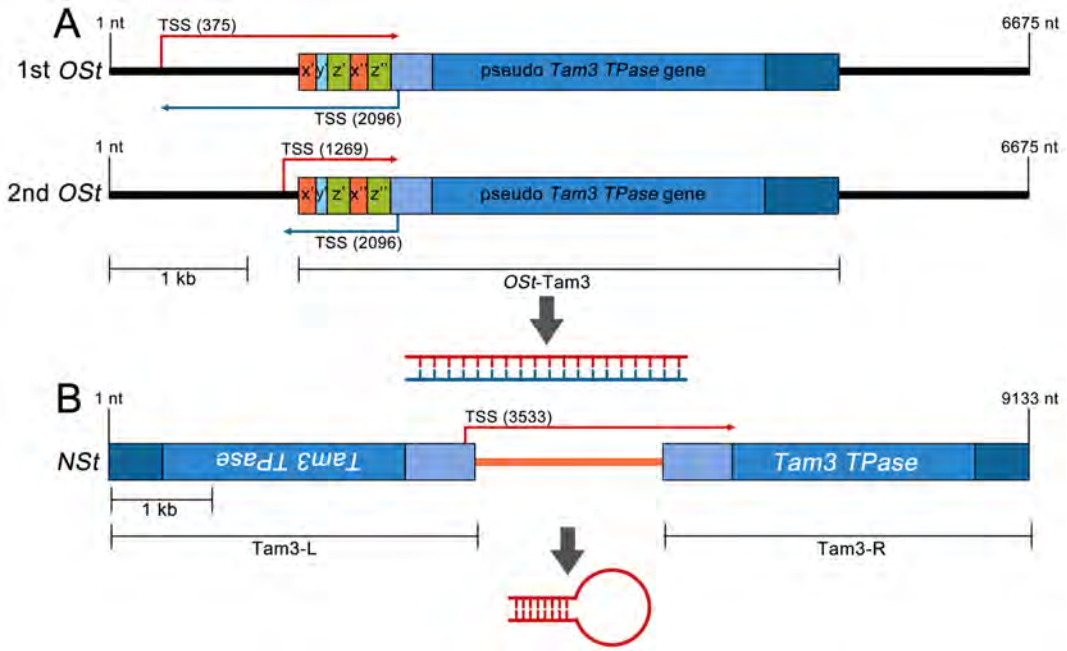


Fig. 5

Possible double-stranded RNAs derived from *OSt* and *NSt*.

A. Possible double-stranded RNAs derived from *OSt*. The two highest combinations of sense and antisense transcriptional start sites were represented in *OSt* (Supplementary Table 3). The transcription on the sense and antisense strands of *OSt* DNA fragment causes the production of sense and antisense transcripts which are paired to form double-stranded RNA. B. Possible double-stranded RNAs derived from *NSt*. One sense transcriptional start site was represented in *NSt*. The transcription starts from the 5' end of Tam3-L and goes through to the 5' end of Tam3-R. The transcript contains two paired parts at the two ends and thus can be folded into stem-loop structure where dsRNA exists in stem part. Red and blue vertical fold arrows represent predicted transcriptional start sites on sense and antisense strands of *OSt* and *NSt*, respectively. The number in parenthesis represents the nucleotide position of TSS from the left side of *OSt* or *NSt*. TSS, transcriptional start site.

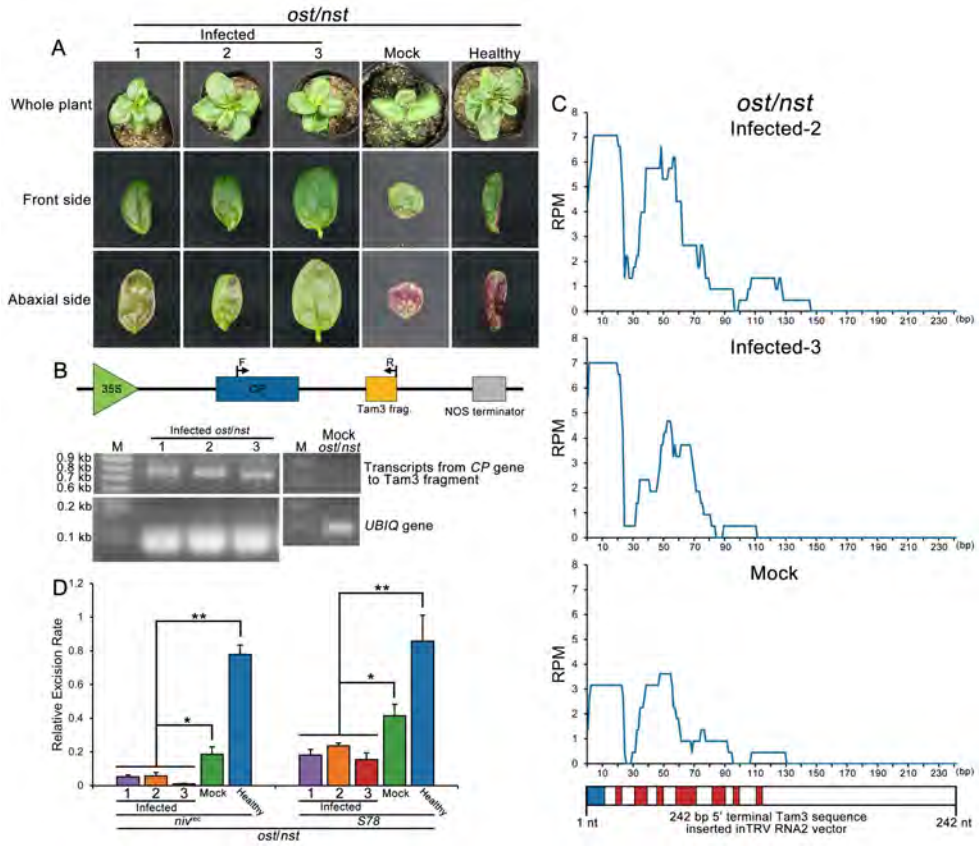


Fig. 6

Tam3 sRNA induction in *nst*/*ost* plants by VIGS.

A. Leaf variegation phenotype in *ost*/*nst Antirrhinum* plants inoculated with TRV carrying 242 bp of 5' terminal Tam3 fragment in sense orientation (TRV-Tam3) and TRV (mock), and without TRV, respectively. 21 days-old *ost*/*nst* plants inoculated with TRV-Tam3, TRV and without TRV were grown at 15 °C for at least two weeks. These plants exhibited different variegation phenotypes on the leaves. B. Detection of transcripts from *CP* gene to the Tam3 fragment in TRV-Tam3-inoculated plants. Tam3 sRNAs production requires the transcription of precusor RNA which is from *CP* gene to inserted Tam3 fragment (Supplementary Fig. 22B).Amplification of *UBIQ* gene was used as a control for cDNA. And amplification of *CP* gene in mock-inoculated plant was used as negative control. Above structure diagram represents the functional section responsible for induction in TRV2 RNA plasmid. Small arrows indicate the positions of primers using for *CP*-Tam3 transcripts. Primer sequences were present in Supplementary Table 4. C. Distributions and amounts of total sRNAs in 5' terminal region of Tam3 sequence in TRV-Tam3-inoculated plants. Aligned sRNAs reads filtered with zero or one mismatch were analyzed. 21, 22, 23 and 24 nt sRNAs were selected respectively and simply combined as total sRNAs. In the structure diagram of 5' terminal region of Tam3 sequence, red and blue squares represent the Terminal Inverted Repeat (TIR) and GCHCG motifs, respectively. RPM: reads per million sequenced reads. D. Relative excision rates of Tam3 copy at *niv*^{rec} and *S78* loci in TRV-Tam3- and mock-inoculated plants and plants without TRV inoculation. Data represents means ± SD. Band intensity was measured by ImageJ. Significant differences were determined by Dunnett's test. Single and double asterisks represent the significant and extremely significant differences, respectively.

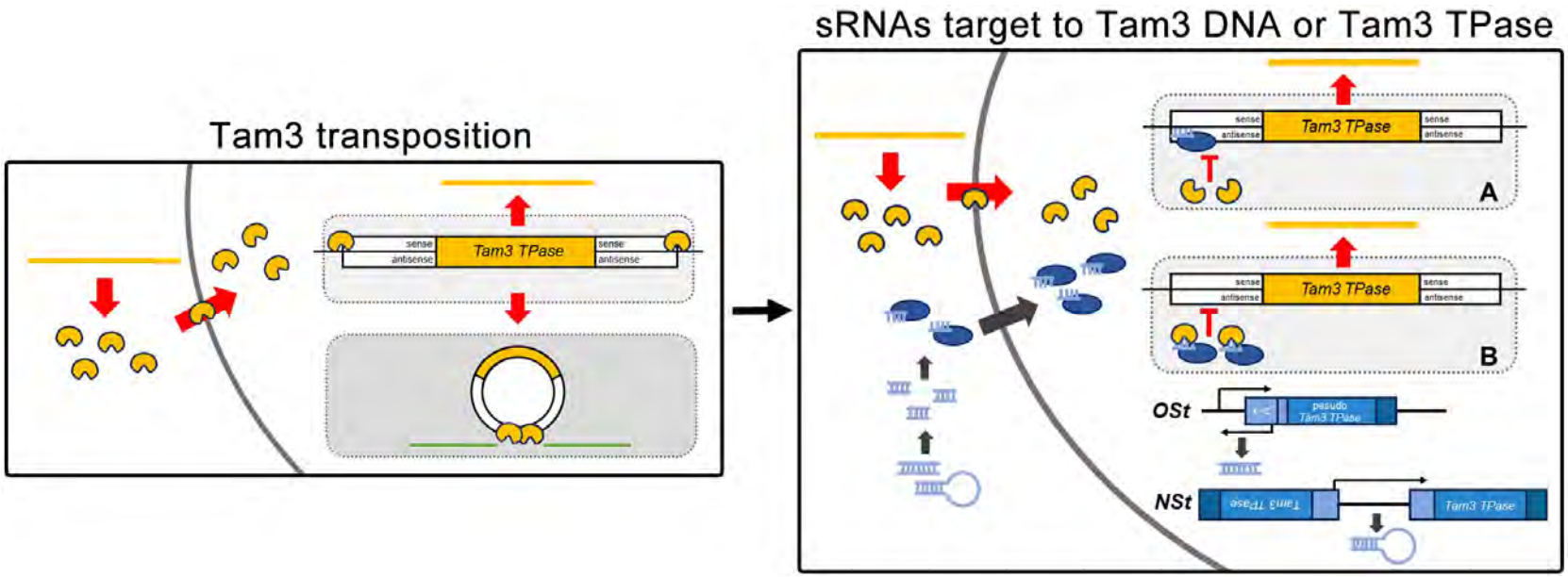


Fig. 7

OSt and *NSt* suppress Tam3 transposition by two possible mechanisms.

Transcription of *OSt* and *NSt* DNA fragments can result in the production of double-stranded RNAs which can be processed into sRNAs. Certain proteins carry these sRNAs and transport them into nucleus. In the nucleus, the sRNAs may bind to the antisense strand of 5' end of Tam3 DNA (A) or interact with Tam3 TPase itself (B) to inhibit the binding between Tam3 TPase and Tam3 DNA, which results in the suppression of Tam3 transposition.